Bioorganic Chemistry 163 (2025) 108681

Contents lists available at ScienceDirect

Bioorganic Chemistry

journal homepage: www.elsevier.com/locate/bioorg

Design, novel one-pot green synthesis, and biological evaluation of pyrazolopyridine-congeners selectively targeting HER2+ breast cancer

Samar M. Mogheith [a], Heba Abdelrasheed Allam [a,*], Manal Abdel Fattah Ezzat [a], Ishaq Khan [b,c], Tamer E. Fandy [d], Dalal Dawud [e], Zakaria Y. Abd Elmageed [e], Amgad Albohy [f,g], Hamed I. Ali [b], Samy Mohamady [f,g,**]

[a] Department of Pharmaceutical Chemistry, Faculty of Pharmacy, Cairo University, Kasr El-Aini Street, 11562 Cairo, Egypt
[b] Department of Pharmaceutical Sciences, Irma Lerma Rangel School of Pharmacy, Texas A&M University, College Station, TX 77843, USA
[c] Massachusetts Institute of Technology, Cambridge, MA, USA
[d] Department of Pharmacology, Texas Tech University Health Sciences Center El Paso, TX, USA
[e] Department of Biomedical Science, Discipline of Pharmacology, Edward Via College of Osteopathic Medicine, University of Louisiana at Monroe, Monroe, LA 71203, USA
[f] Department of Pharmaceutical Chemistry, Faculty of Pharmacy, The British University in Egypt, Cairo 11837, Egypt
[g] Drug Research and Development Group (DRD-G), The British University in Egypt, Cairo 11837, Egypt

ARTICLE INFO

Keywords:
Pyrazolopyridines
Antitumor
HER2 inhibitors
Docking
Molecular dynamics

ABSTRACT

Breast cancer (BC) is among the most prevalent and most aggressive cancer types affecting females. Several targets were investigated to tackle this problem, among them HER2 receptors are one on the most studied targets. In this study we report the synthesis of 18 different pyrazolopyridine (**3a–r**) derivatives using a novel green one-pot method. The synthesized compounds were screened against NCI 60 human tumor cell panel at single concentration. The six top compounds (**3c**, **3d**, **3f**, **3l**, **3m** and **3o**) were followed up by plotting their IC_{50} values and selectivity indices against different cancer types. Kinase profiling for the top two compounds (**3f** and **3o**) was done against 20 different kinases and showed that they have selective inhibition of HER2 (with −88 and − 75 % inhibition) comparable to Tucatinib (−90 % inhibition). In addition, Annexin V PI/FITC apoptosis assay using BT474 cell lines on compounds **3l**, **3o** and **3f** demonstrate the target specificity of our most potent compounds towards HER2 + ve harboring cells. In vivo antitumor activity of compound **3f** on BC xenograft mouse model demonstrates that the recorded tumor size over the course of study was significantly reduced by 19.45 % when mice treated with **3f** compared to 38.6 % reduction when treated with lapatinib. Finally molecular docking and molecular dynamics studies were used to investigate and understand the potential binding modes and interactions between the synthesized compounds and HER2 on the molecular level. In summary, this study presents the synthesis of this new promising scaffold as anti breast cancer medication using a novel green one-pot method.

1. Introduction

The ErbB family of receptor tyrosine kinases include HER1 (EGFR), HER2, HER3, and HER4—transmembrane proteins with intracellular kinase domains and extracellular ligand-binding regions. [1] Unlike EGFR, HER2 lacks a known ligand, remaining constitutively active. [2] HER2 overexpression, found in 20–30 % of breast cancers (BC), is associated with poor prognosis. [3] It is also overexpressed in various other solid tumors including uterine, gastric, and colorectal cancers, though at varying frequencies. [4] Additionally, recurrent somatic mutations in ERBB2 have been observed across multiple malignancies. [5]

HER2 possesses the highest catalytic activity among the HER family and remains constitutively active due to its ligand-independent conformation. [6] This makes it a key partner in heterodimerization with other EGFR family members, triggering autophosphorylation and activating oncogenic signalling cascades. [7] Targeting HER2 has yielded promising results in BC treatment, notably with the monoclonal antibody trastuzumab (Herceptin). [8] In female patients with BC who exhibit

* Corresponding author.
** Corresponding author at: Department of Pharmaceutical Chemistry, Drug Research and Development Group (DRD-G), Faculty of Pharmacy, The British University in Egypt, El-Sherouk City, Cairo 11837, Egypt.
E-mail addresses: heba.abdelkhalek@pharma.cu.edu.eg (H.A. Allam), samy.mohamady@bue.edu.eg (S. Mohamady).

https://doi.org/10.1016/j.bioorg.2025.108681
Received 29 March 2025; Received in revised form 8 June 2025; Accepted 9 June 2025
Available online 12 June 2025

HER2 overexpression and/or amplification, HER2-targeted treatments are beneficial. The first anti-HER2 mAb, trastuzumab, was initially developed in 1990. It inhibits HER2 signalling through a number of mechanisms, including antibody-dependent cellular cytotoxicity (ADCC), receptor internalization and/or degradation, and PI3K–AKT signalling pathway inhibition. [9] Adjuvant therapy with trastuzumab has been shown to improve survival for women with HER2-positive BC when given for a year, both in early stages of the illness and in advanced metastatic stages. [10–13] Patients with HER2-positive NSCLC have also participated in a number of phase II clinical trials, some of which have been successful, despite the small number of patients involved. [14,15] BC Patients with HER2 gene amplification and protein overexpression, constituting about 20 % of all BC patients, had a worse prognosis prior to the FDA's approval of trastuzumab for use in treatment. [16] In addition, HER2-positive BC have shown a markedly improved prognosis when treated with small molecules and other antibodies targeting HER2, such as lapatinib, pertuzumab, and the recently approved compound ado-trastuzumab emtansine. [11,17,18]

HER2-targeted therapies have shown strong efficacy in HER2-positive BC. For instance, combining lapatinib with capecitabine extends progression-free survival compared to trastuzumab alone. [19] Nonetheless, resistance can develop due to mechanisms such as HER2 heterodimerization, MUC4 overexpression, or generation of truncated HER2 (p95) lacking trastuzumab binding. [20,21] Several HER2 inhibitors—including trastuzumab, lapatinib, pertuzumab, T-DM1, afatinib, and neratinib—have received approval, with afatinib also indicated for EGFR-mutant NSCLC. [22]

The first dual EGFR/HER2 inhibitor, lapatinib (Fig. 1), was approved by the FDA in 2007 to treat BC. For the dual inhibition of EGFR and HER2, its bulky 4-benzyloxyaniline substituent is necessary while smaller anilines only inhibit EGFR, such as 3-ethynylaniline in erlotinib and 3-chloro-4-fluoro-aniline in gefitinib. [23] Lapatinib attaches itself to the inactive closed conformation of EGFR, causing the αC-helix to move "out" and granting the 3-fluorobenzyloxy group entry to the hydrophobic back pocket. [24,25] Comparing this extra binding in the back pocket to gefitinib and erlotinib, which do not have access to the rear pocket, reveals a longer duration of inhibition for combined EGFR/HER2 inhibition. [26] Aside from potentially introducing off-target effects including diarrhea and dermatitis, targeting other members of the HER family, such as EGFR (HER1), does not functionally decrease HER2 signalling. [27] Furthermore, inhibiting EGFR or HER4 does not functionally decrease HER2 signalling in BC cells that overexpress HER2, which means that it does not stop tumor cell proliferation or survival. [28,29] Notably, lapatinib has another significant side effect as an EGFR inhibitor as it can cause excruciating skin rashes and diarrhea. Skin toxicity is commonly exhibited as mild to severe papulopustular rash in most patients (45–100 %) using EGFR inhibitors. [30–32] Physical and psychosocial difficulties are revealed by these side effects, especially in female BC patients.

The capacity of small-molecule TKIs to inhibit numerous kinases including p95 HER2 (a highly active truncated form of HER2 lacking the majority of the extracellular domain) offers potential benefits over mAb treatments. [33,34] Correspondingly, TKIs have a stronger ability to cross the blood-brain barrier and a larger therapeutic potential against brain metastases. [35] They also have reduced cardiac toxicities, which are typically associated with mAb therapies. [17,18]

Pyrazolo[4,3-*b*]pyridine is widely recognized for its ability to inhibit several kinases, including anaplastic lymphoma kinase (ALK). [36], protein kinase B (Akt) [37], Aurora-A kinase [38], hepatocyte growth factor receptor (HGFR) [39], epidermal growth factor receptor (EGFR) [40], mitogen-activated protein kinase (MAPK) [41], cyclin-dependent kinase1 [42] and 2 (CDK1/CDK2) [43], cyclin-dependent kinase 5 (CDK5) [44], cyclin-dependent kinase (CDK8) [45], B-RafV600E kinase [46], cAMP-dependent protein kinase and cGMP-dependent protein kinase pathways [47], fibroblast growth factor receptor (FGFR) [48], TASK3 Kinase [49], activation of adenosine 5′-monophosphate-

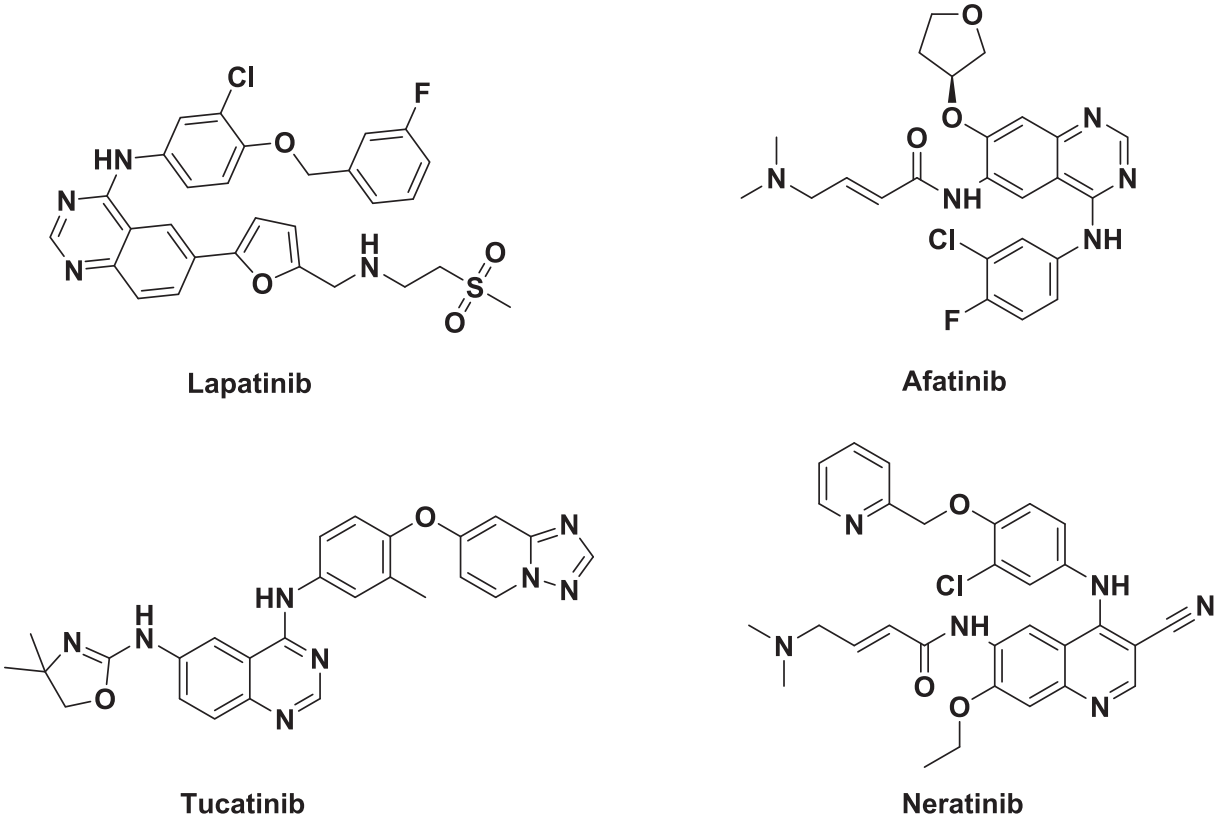

Fig. 1. Chemical structures of currently marketed anti-HER drugs.

activated protein kinase (AMPK) [55], ataxia-telangiectasia and Rad3-related kinase (ATR) [50], glycogen synthase kinase-3 (GSK-3) [51], [52], also, activin-like kinase 5 (ALK5) [53]. These finding shows the potential importance of this scaffold in the design and synthesis of novel kinase inhibitors. Synthetic approaches for the synthesis of pyrazolo [4,3-*b*]pyridine unsubstituted at position 1 are limited and require multistep reactions leading to poor yield [54] Herein, we report a novel one-pot synthesis of pyrazolo[4,3-*b*]pyridine from simple starting agents namely, aldehyde, hydrazone and cyanoketones. The new synthesized series was designed by exploiting pyrazolo[3,4-*b*]pyridine-5-carbonitrile block as a purine bio-isostere to fit in the adenine region of the ATP binding pocket. Moreover, hydrophobic warhead and lipophilic tail were introduced to occupy the hydrophobic region I and II inside the pocket (Fig. 2), thus enabling them to occupy desired key pockets that localized nearby the ATP binding site to surmount kinase drug selectivity hurdle and provide more potent targeted treatments. Based on that we decided to limit our studied variables in this initial study by limiting the hydrophobic warhead (Substituent X) in Fig. 2 to halogens (Cl and Br). This will help us to understand the effect of modifications done on the lipophilic tail (Ar). Several substituents on the aromatic ring were studied including fluoro and trifluoromethyl moieties as well as methoxy groups at different position. In addition, thiophene ring was also used as a bio isostere of the phenyl ring.

2. Results and discussion

2.1. Chemistry

In our interest in the chemistry of aldehyde hydrazones, we have previously reported their utilization in a novel one-pot synthesis of diaryl pyrazoles [55,56] through their reaction with 2-bromoacetophenones (Scheme 1, pathway a). However, the reaction of 1.2 equiv. aldehyde hydrazones with 1.0 equiv. 2-cyanoacetophenones gave the corresponding triaryl-1*H*-Pyrazolo [3,4-b]pyridine derivatives **3e**, **3g** in 40 % and 42 % yields respectively (Scheme 1, pathway b). Structure of compounds **3e**, **3g** were confirmed by X-ray crystallography (Fig. 3 and Supp. Info. S5 and S6), as well as ^{1}HNMR, and ^{13}C NMR (Experimental section as well as Supp. Info S1). For example, compound **3e** exhibited two singlet peaks at δ 3.40 (s, 3H, OCH_3) and 3.82 (s, 3H, OCH_3). The aromatic region of the spectrum corresponds to a sum of 11 protons, where the two doublets at δ 7.83 (d, 2H, Ar—Hs, J = 8.32 Hz) and 7.90 (d, 2H, Ar—Hs, J = 8.40 Hz) corresponds to ortho positions of the halogen carryings rings. While 4 protons at meta position of the halogen carrying rings showed one doublet at δ 7.33 (d, 2H, Ar—Hs, J = 8.16 Hz), and double doublet at δ 6.98 (dd, 3H) overlapping the doublet of proton at 5-position of dimethoxy ring. Peaks at δ 6.82(s, 1H), 7.07 (s, 1H) correspond to two protons at the dimethoxy ring. The pyrazole 1H proton appeared downfield at δ 14.59 (s, 1H, NH exchanged with D_2O) that was exchangeable with D_2O. ^{13}C NMR spectrum showed two peaks at δ 55.72 ($O\underline{C}H_3$), 56.30 ($O\underline{C}H_3$) of the dimethoxy groups and the rest of peaks at δ 101–159 ppm. Optimization of reaction conditions revealed that optimum ratio of hydrazone to cyanoketone is 1: 1.6 that resulted in maximum obtained yield (62–78 %).

The proposed reaction mechanism for the formation of 1*H*-Pyrazolo [3,4- b]pyridines (Fig. 4) starts with the condensation of cynoacetophenone **1** with hydrazone **2** in presence of aqueous acid (3 M HCl) under reflux to form intermediate **3**. Under the aqueous acid conditions, compound **3** undergo immediate hydrolysis to form hydrazone **4** and aldehyde **5**. Intramolecular cyclization of **4** forms 3-aminopyrazole **6.** Simultaneously, **5** reacts with one more mole of cyanoacetophenone **1** to form the arylidene cyanoketone **7**. final product could be formed by two possible routes. Route a: cyanoketone **7** undergoes Michael addition with 3-aminopyrazole **6** to give intermediate **8**, which condenses to **11**, which is then oxidized by the presence of DMSO to give the final product. On the other hand, in route b condensation of 3-aminopyrazole **6** with cyanoketone **7** to give intermediate **9** followed by intramolecular Diels-alder cyclization to give intermediate **11** which again oxidizes to final product. We found that this oxidation step can occur without the need for DMSO however with much lower yields.

With the optimized procedure in hand, we proceed to synthesize the library of compounds as shown in Scheme 2.

2.2. Biological evaluation

2.2.1. In vitro single-dose (10 μM concentration) screening against NCI 60 human tumor cell panel

Single-dose testing was carried out at a concentration of 10 μM, which is one 10th the highest concentration used in the 5-dose testing protocol and is done against all sixty cell lines, representing nine tumor subpanels. The protocol and data analysis were carried out by NCI's Developmental Therapeutics Program (DTP). The results for each compound were expressed as a percentage of cell growth of the treated cancer cells compared to untreated control cells and relative to the time zero number of cells. Accordingly, the results enable the detection of both lethality (negative values between −100 % and zero) and growth inhibition (positive values between zero and 100 %). A value of 100, for instance, denotes no growth inhibition. A value of 40 indicates a 60 % growth inhibition. A value of zero indicates that there was no cell growth at all during the assay. Forty percent lethality would be implied by a value of −40. Cells are considered dead at a value of −100. As shown in Fig. 4, tested compounds demonstrated varied patterns of

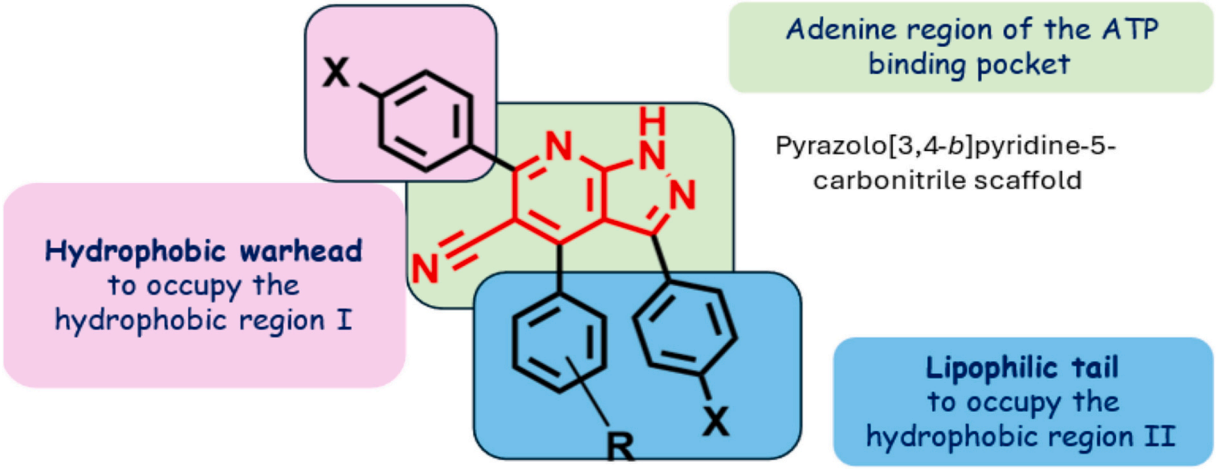

Fig. 2. Design of the targeted compounds **3a–r**.

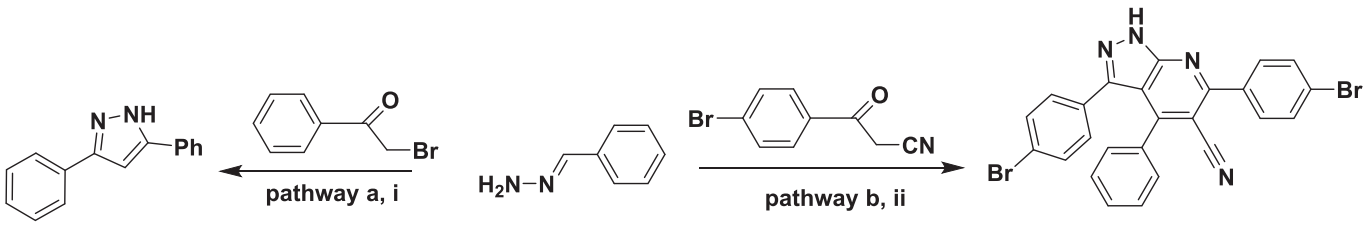

Scheme 1. Synthesis of 4-substituted-*3,6-Bis(4-bromophenyl)-1H-pyrazolo[3,4-b]pyridine-5-carbonitriles (**3e** and **3g**):. Reagent and reaction conditions:* (i): Ethanol, HCl, DMSO, reflux, 48 h; (ii): Ethanol, HCl, DMSO, reflux, 72 h.

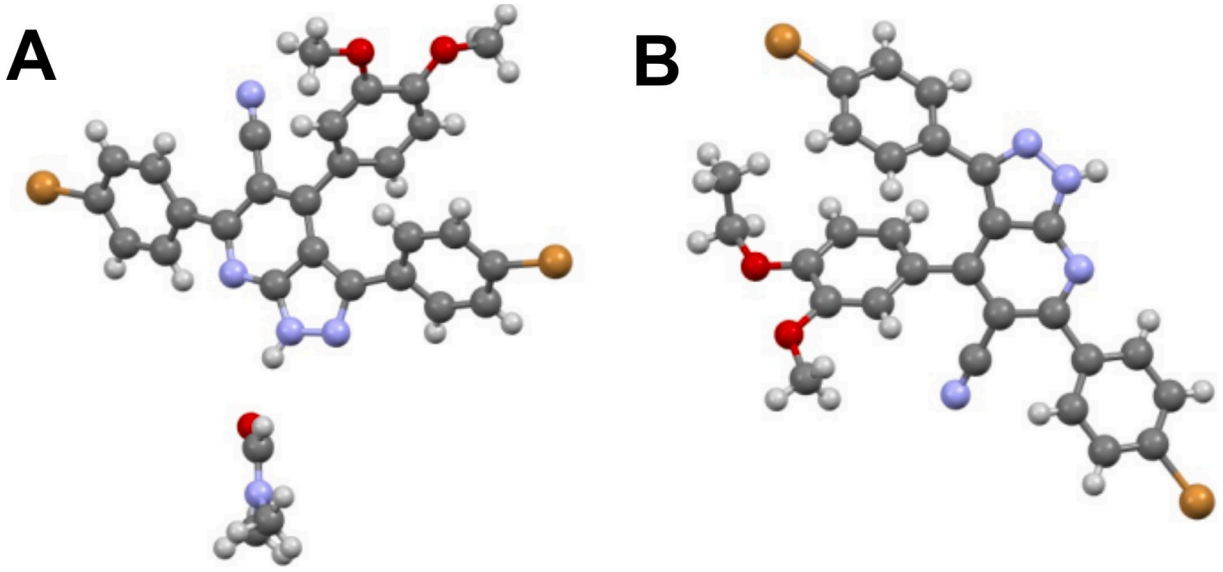

Fig. 3. X-Ray crystal structures. A. Compound **3e** with a co-crystallized DMF molecule; B. Compound **3g**. Grey, white, blue, red and orange represents carbon, hydrogen, nitrogen, oxygen and bromine, respectively. (For interpretation of the references to colour in this figure legend, the reader is referred to the web version of this article.)

growth inhibition as well as cytotoxicity against various NCI cell panels.

Interestingly, compounds **3c**, **3m**, **3d**, **3l**, **3o**, and **3f** as evidently displayed in Fig. 5, demonstrated mean cell growth inhibition and lethality in the ranges of (14.67–42.97 %) and (−18.38 - -38.52 %), respectively. The DTP program at NCI chose these potent compounds for additional 5-dose screening using the mean growth percent of 50 % as the minimal threshold for inhibition. Compounds **3c**, **3d**, **3f, 3l**, **3m**, and **3o** showed broad spectrum cell growth inhibition and lethality against Leukemia (a lethality up to −48.96 %) and non-small cell lung cancer (a lethality up to −77.46 %). Also, a lethality up to −92.28 % was recorded for colon cancer, a lethality up to −92.04 % for CNS cancer, a lethality up to −100.0 % for melanoma, a lethality up to −41.81 % for ovarian cancer, a lethality up to −72.81 % for renal cancer, and a lethality up to −70.93 % for BC. These compounds demonstrated a high degree of lethality against melanoma, colon, CNS, and non-small cell lung cancer cell lines. While broad-spectrum cell growth inhibition was demonstrated by compounds **3g** and **3h** against the five BC cell lines, the MCF7 and T-47D BC cell lines were selectively inhibited by compounds **3r**, **3g**, and **3p**. Furthermore, compounds **3l** and **3h** demonstrated a strong inhibitory impact against the majority of non-small cell lung cancer cell lines. They inhibit 6 out of 9 cell line called A549/ATCC, EKVX, HOP-92, NCI-H226, NCI-H460, and NCI-H522. **3g** and 3q on the other hand, displayed a selective inhibitory impact on the EKVX cell line.

While compounds 3q and 3i displayed narrow-spectrum inhibition against three of the utilized leukemia cell lines, compounds 3r, **3l**, 3p, **3g**, and **3h** demonstrated broad-spectrum inhibition against five to six leukemia cell lines. Compound **3r, 3g, and 3q**, exhibited significant growth inhibition against four out of six tested colon cancer cell lines namely HCT-15, HT29, KM12, and SW-620.

The Ovarian Cancer cell lines were inhibited by compound **3h** in a broad-spectrum manner, whereas compound **3l** inhibited the Ovarian cell lines in a narrow-spectrum manner against three cell lines. The PC-3 prostate cancer cell line was selectively inhibited by compounds **3r**, **3g**, **3l**, **3q**, **3h**, and **3p**.

2.2.2. In vitro five-dose full NCI 60 cell panel screening

Six compounds, out of the nineteen initially screened compounds at a single high dose (10 μM), were chosen to be screened by five-dose concentration against the entire NCI 60 cell panel. In the single-dose screen, compounds **3c**, **3m**, **3d**, **3l**, **3o**, and **3f** displayed notable growth inhibitions. The criteria for effectively capturing these six compounds and advancing them to the 5-dose anti-proliferative activity were based on a detailed examination of previous DTP screening data. Five different ten-fold concentrations of the tested chemicals (0.01, 0.1, 1.0, 10, and 100 μM) were used in this assay.

For every compound in comparison to every cell line, three dose-response parameters (GI_{50}, TGI, and LC_{50}) were calculated (Table 1). GI_{50} (growth inhibition of 50 %), is the concentration of the test compound that results in a net cell growth inhibition of 50 %. LC_{50} (lethal concentration of 50 %, cytotoxic activity), which is the drug concentration that results in a 50 % loss of initial cells (not growth) at the end of the 48-h incubation period, and TGI (total growth inhibition), which is the drug concentration that results in a full growth inhibition.

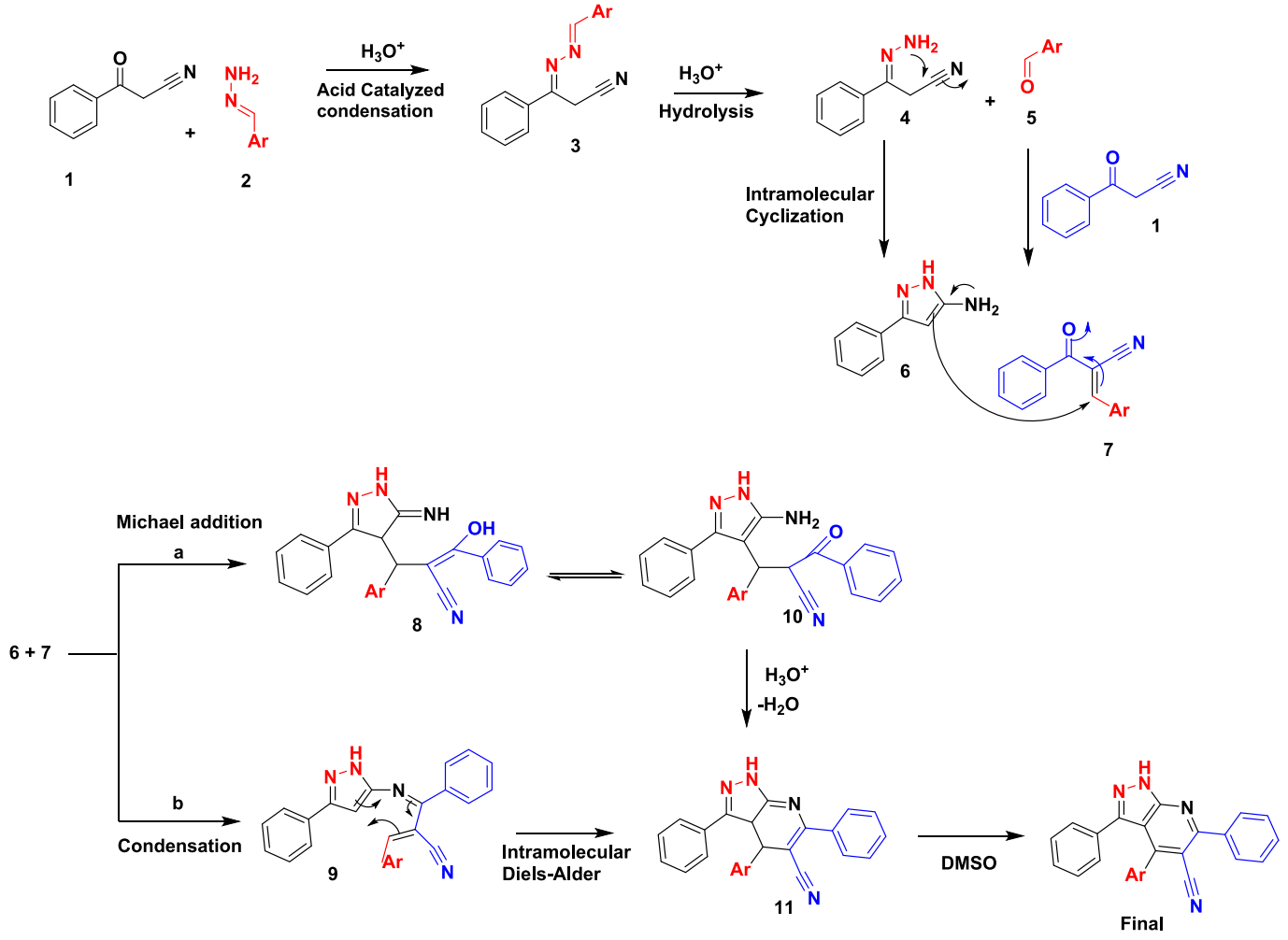

Fig. 4. Proposed mechanism for the one-pot formation of 3,4,6-triaryl-1*H*-pyrazolo[3,4-*b*]pyridine-5-carbonitrile.

2.2.3. Potency of the test compounds towards 9 subpanels of NCI 60 cell lines

With GI_{50} values ranging from 1.4 to 4.7 μM, test compounds **3f**, **3m** and **3o** demonstrated excellent anticancer activity against most of the NCI 60 cell lines representing nine different subpanels. The best inhibitions were identified against leukemia, CNS, and BC cell lines, with average GI_{50} values of (1.9, 2.3, and 2.3 μM), (2.5, 2.3, 2.1 μM), and (2.3, 2.1, and 1.9 μM), respectively. Compounds 3c, 3d, and **3l** displayed moderate anticancer efficacy against colon cancer and leukemia to a lesser extent, with GI_{50} values ranging from 1.89 to 21.2 μM and average values of (6.06, 4.07, 9.43 μM) and (4.02, 2.41, and 5.05 μM), respectively.

Similar results were obtained with compounds **3f**, **3m** and **3o** against ovarian and renal cancer, with GI_{50} values ranging from 1.81 to 4.7 μM and average GI_{50} values of (2.51, 2.97 and 2.8 μM), (2.73, 2.72 and 2.8 μM), respectively. When it comes to sensitivity to specific cell lines, compound **3o** and **3f** exhibited high activity against leukemia-HL-60 (TB) (GI_{50} = 1.89 and 1.2 μM, respectively), whereas compound **3m** demonstrated strong activity against Leukemia SR (GI_{50} = 1.69 μM). Furthermore, a variety of compounds, including **3c**, **3m**, **3d**, **3l**, **3o**, and **3f**, with corresponding GI_{50} values of 2.85, 2.53, 3.39, 3.42, 2.08, and 1.77 μM, significantly suppressed the growth of BC T-47D cells.

With GI_{50} values of 1.5, 1.6, and 2.3 μM, respectively, it has been demonstrated that the non-small cell lung cancer HOP-92 cells are extremely susceptible to the effects of compounds **3m**, **3d**, and **3l**. Similarly, compound **3f** inhibited NCI-H23 cells by GI_{50} of 1.9 μM, compounds **3m** and **3f** showed significant GI_{50} against NCI-H522 with GI_{50} of 2 and 2.5 μM, respectively. Both **3c** and **3d** significantly inhibited the prostate cancer PC-3 cell, with GI_{50} values of 2.8 and 1.9 M, respectively. Regarding CNS cancer cell lines, SNB-75 cells were inhibited by **3c**, **3m**, **3o**, and **3f** with GI_{50} equal to 1.14, 1.75, 2.15 and 1.68 μM, respectively. Similarly, compounds **3o** and **3f** demonstrated substantial GI_{50} against SF-295 and SF-539 cells equal to (1.69, 1.62 μM) and (1.63, 1.58 μM) respectively. Versus Colon cancer-COLO 205, compound **3m** exhibited high inhibitory activity with GI_{50} equal to 1.7 μM, as well, compound **3c**, **3m**, **3d**, **3l**, **3o**, and **3f** exhibited great inhibition against HCT-15 cells with GI_{50} equal to 3.1, 2.5, 3.2, 4.1, 1.9 and 1.86 μM respectively.

2.2.4. Selectivity of the test compounds towards 9 subpanels of NCI 60 cell lines

The selectivity profile of the six compounds tested, **3c**, **3d**, **3f**, **3l**, **3m**, and **3o**, against NCI-60 human tumor cell lines at five dose levels was calculated. The selectivity ratio (S) for a test compound was calculated by dividing its average GI_{50} towards a full panel of NCI 60 cell lines (MID-all) by its average GI_{50} towards cell lines of a specific subpanel (MID); a larger value denotes better selectivity. According to this criterion, all the test compounds showed certain selectivity profile towards Leukemia (S: 1.13–2.58) and BC (S: 1.03–1.52).

To a lesser extent, test compounds **3m** and **3d** demonstrated minor selectivity (S: 1–1.08) towards non-small cell lung cancer, compounds **3c**, **3m**, **3d**, **3l** and **3o**, (S: 1.05–1.71) against colon cancer, compounds **3o and 3f** (S: 1.14–1.19) against CNS cancer, and compounds, 3c, **3m**, 3o, and 3f (S: 1.06–1.16) against melanoma. Regarding Leukemia and

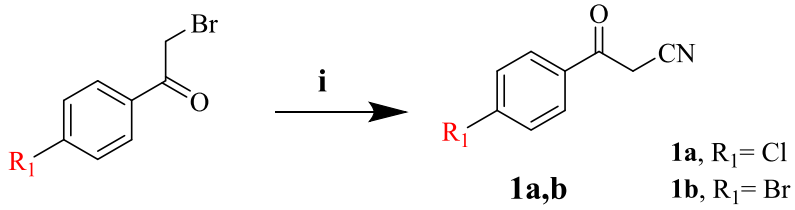

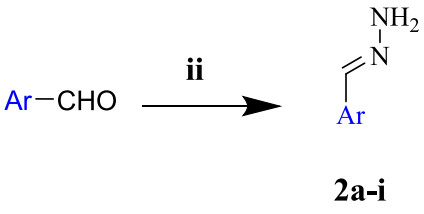

Ar= C_6H_5,4-F C_6H_4, 4-$OCH_3C_6H_4$, 4-$CF_3C_6H_4$, 3,4-dimethoxy C_6H_3, 3-OH,4-$OCH_3C_6H_3$, 3-OCH_3,4-$OCH_2CH_3C_6H_3$, 3,4,5-trimethoxy C_6H_3, 2- thiophenyl

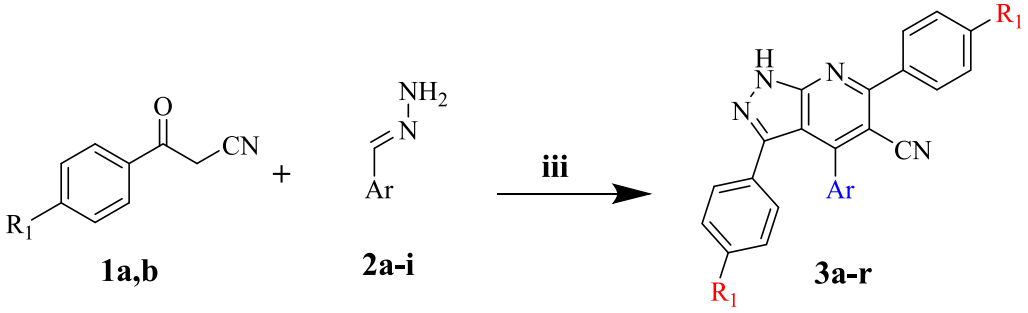

Comp. no.	R_1	Ar	Comp. no.	R_1	Ar
3a	Br		3j	Cl	
3b	Br	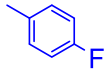	3k	Cl	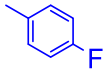
3c	Br	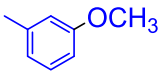	3l	Cl	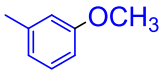
3d	Br	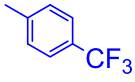	3m	Cl	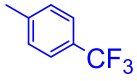
3e	Br	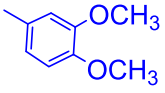	3n	Cl	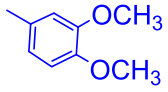
3f	Br	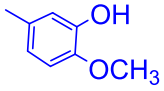	3o	Cl	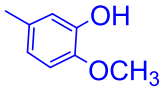
3g	Br	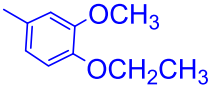	3p	Cl	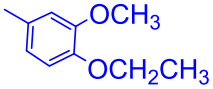
3h	Br	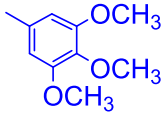	3q	Cl	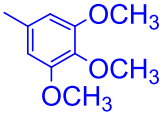
3i	Br		3r	Cl	

Scheme 2. Synthesis of target 4-substituted-*3,6-Bis(4-bromophenyl)-1H-pyrazolo[3,4-b]pyridine-5-carbonitriles. Reagents and reaction conditions*, (**i**): KCN, MeOH, rt., 3 h; (**ii**): $N_2H_4.H_2O$ 99.9 %, absolute EtOH, reflux, 3 h; (**iii**): 3 M HCl, reflux, 72 h.

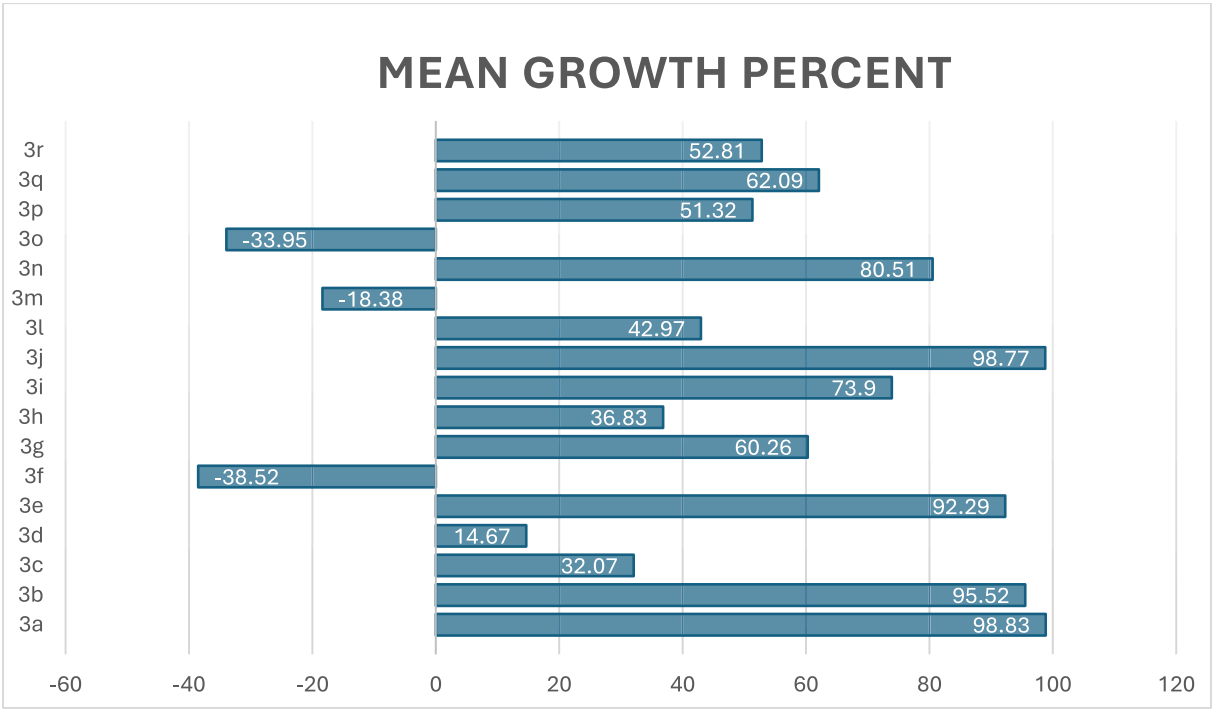

Fig. 5. The percent of growth rate for tested compounds at single 10 μM concentration to examine anticancer activities against NCI 60 human tumor cell panels.

BC the whole six compounds 3c, **3m**, 3d, **3l**, 3o, and 3f showed selectivity profile (S: 1.13–2.58) and (S: 1.03–1.52) respectively as shown in Table 1 and represented in Fig. 6.

In terms of the selectivity against a specific subpanel of NCI-60 cell lines, compounds **3c**, **3m**, **3d**, **3l**, **3o**, and **3f** were discovered to be most significantly selective towards Leukemia cells with selectivity ratio (S) of 2.58, 1.28, 2.19, 2.36, 1.15, and 1.13 respectively. Additionally, compounds **3c**, **3m**, **3d**, and **3l** were found to be most selective towards Colon cancer subpanel with (S) of, 1.71, 1.05, 1.3, 1.26 respectively. Moreover, compounds **3c** and **3d** were found to be the most specific towards Prostate cancer with (S: 1.24–1.42), respectively. Furthermore, Against Ovarian cancer, only compound **3c** exhibited high selectivity with (S: 1.07).

2.2.5. In-vitro protein kinase inhibition assay

2.2.5.1. Kinase profiling at single concentration of 10 μM against 20 different kinases including HER2. KINEXUS Bioinformatics Corporation, Vancouver, British Columbia, Canada, assessed the protein kinase profiles of 2 compounds (**3f** and **3o**) against a panel of 20 protein kinases utilizing the ADP-Glo assay technique. Tucatinib was used as a reference compound. Using the standardized assay methodology described in the experimental portion, this test was carried out at a concentration of 10 μM. In this study, the compound's ability to inhibit target activity was given a negative (−) value while its ability to activate target activity was given a positive (+) value. Only activity changes of over 25 % relative to the control were considered significant. HER2 was specifically targeted by **3o** and **3f**, which inhibited it with an inhibition percentage of −79 % and − 88 %, respectively. None of the other kinases that were examined were inhibited.

Tucatinib (Tukysa®) was the reference compound utilized in this assay. It is a small molecule used to treat BC that is HER2-positive. Tucatinib inhibited three kinases, including HER2, HER4, and EGFR, by more than −86 % in this experiment. It also slightly inhibited BTK (−40 %) and MET (−53 %). None of the other kinases that Tucatinib was tested on displayed any discernible inhibitions.

2.2.5.2. Determination of IC_{50} of 3o and 3f against HER2 kinase. Two compounds (**3f** and **3o**) were tested at 10 concentrations (ranging from 0.05 μM to 250 μM) against HER2 protein kinase using the ADP-Glo assay method to determine their IC_{50} values. In this assay, recombinant protein kinases were cloned, expressed, and purified using proprietary methods. In this study, triplicate measurements were also taken with the control substrate. Inhibition values were obtained by determining the change in Relative Light Units (RLU) between the control substrate (average) and the increasing concentration of compound added to the reaction. The inhibition values obtained for the two compounds ranged from nil at the lowest concentrations up to −89 % at the 250 μM concentration.

The inhibition values in this experiment were lower than the single measurement at 10 μM concentration (Table 3). Previously, these two compounds showed 75 and 88 % inhibitions at 10 μM. In this study, 3o and 3f reached −60 and − 57 % inhibition only at 250 μM. Differences are likely due to experimental variations, such as different ATP batches, protein kinase preparations, and reagent lots. Additionally, the control substrate had lower counts in the first study, making changes appear greater. Different batches of the compounds also contributed to the variation. The IC_{50} values for the two compounds were extrapolated from the data and determined to be 199 μM for **3o** and 215 μM for **3f**. (Table 4).

2.2.6. Antiproliferative activity and antimigratory assays with breast cancer cell lines

The antiproliferative effects of our newly synthesized compounds were evaluated using an MTT assay against three distinct HER2-expressing BC cell lines (BT474, BT549, and ZR-75-30). Lapatinib, an FDA-approved dual EGFR/HER2 tyrosine kinase inhibitor, served as a positive control. All our compounds revealed statistically significant potent antiproliferative activities against the tested HER2 + BC cells (BT474, BT549 and ZR-75-30) with IC_{50}s ranging from lower to submicromolar levels (Table 5). Interestingly, when tested against human metastatic triple-positive BC cells (BT474), all of the synthesized compounds showed strong antiproliferative effects, with an IC_{50} ranging from 323.2 to10503 nM. Compounds **3r**, **3h**, **3n**, **3i**, and **3f** have the best

Table 1
In vitro NCI-60 human tumor cell line anticancer screening data for compounds **3c**, **3d**, **3f**, **3l**, **3m**, and **3o** at five dose level in μM concentration expressed as GI_{50} (stands for growth inhibition of 50 %) and TGI (total growth inhibition).

	3c		**3d**		**3f**		**3l**		**3m**		**3o**	
	GI_{50}	TGI	GI_{50}	TGI	GI_{50}	TGI	GI_{50}	TGI	GI_{50}	TGI	GI_{50}	TGI
Leukemia												
CCRF-CEM	6.04	100	3.05	13	2.8	100	6.56	100	2.18	6.57	2.93	10
HL-60 (TB)	3.16	100	2.03	6.13	1.21		4.77	43.5	1.79	4.79	1.89	100
K-562	3.33	100	2.61	10.3	2.46	100	4.01	78.6	2.09	5.91	2.31	100
MOLT-4	3.07	100	1.89	6.02	2.19	100	3.45	49.2	1.72	6.12	2.29	100
RPMI-8226	3.44	100	2.35	10.4	2.22	6.29	4.44	100	1.93	6.27	2.08	5.28
SR	5.09	100	2.5	7.71	2.89	100	7.09	50.3	1.69	4.42	2.43	
Non-small cell lung cancer												
A549/ATCC	9.9	100	4.62	100	3.2	13.1	15.1	100	3.45	12	3.21	12.9
EKVX	8.64	100	3.05	27.3	2.69	13.2	11.8	100	2.71	11.4	2.92	11.8
HOP-62	23	100	14.1	44.7	2.53	7.4	16.4	80.7	3.06	9.83	2.96	10.4
HOP-92	2.46	37.8	1.65	4.73	2.21	8.84	2.35	9.24	1.57	4.37	2.12	7.89
NCI-H226	5.82	100	3.07	18	3.18	17.8	11.9	49.1	2.37	8.97	3.71	15.3
NCI-H23	8.29	100	4.31	100	1.96	6.47	13.6	100	2.24	7.68	2.84	9.83
NCI-H322M	43.2	100	5.62	41	3.39	18.1	24	100	2.4	13.2	3.58	15.7
NCI-H460	6.73	100	3.62	19.4	3.05	10.5	13.5	46.7	2.08	4.57	2.77	10.1
NCI-H522	6.6	100	3.78	36.9	2.24	6.37	16.1	92.7	2.03	5.68	2.54	8.84
Colon cancer												
COLO 205	7.7	21.3	3.88	15.9	4.33	15.1	11.3	25.2	1.71	3.24	4.4	16
HCC-2998	4.87	73.5	5.27	27.1	2.75	8.39	6.14	31	2.29	5.36	2.77	8.41
HCT-116	4.05	100	3.42	73.2	2.93	11.4	4.66	26.2	1.61	3.73	3.01	10.7
HCT-15	3.19	16.2	3.29	19.1	1.86	4.19	4.16	27.8	2.57	10.4	1.97	4.87
HT29	3.68	34.3	3.84	35.7	2.65	13.7	9.76	29.8	2.77	10.9	2.94	11.7
KM12	6.95	100	4.4	26.8	3.57	17.8	8.81	100	2.49	8.32	3.38	13.1
SW-620	12	100	4.39	100	3.68	15.3	21.2	100	2.76	10.8	3.36	14
CNS cancer												
SF-268	18	100	7.91	100	3.17	14	14.8	100	2.93	11.5	3.21	14.4
SF-295	8.86	71.5	2.61	10.1	1.62	3.27	12.1	33	2.62	8.3	1.69	3.55
SF-539	8.77	100	5.35	22.2	1.58	3.33	8.28	25.9	1.85	3.76	1.63	3.71
SNB-19	19.4	100	4.53	33.3	3.19	13.4	20	100	3.38	14.7	3.24	13.5
SNB-75	1.14	100	12.6	43.9	1.68	10.3	12.7	64.3	1.75	6.59	2.15	9.16
U251	7.48	100	6.23	62.4	1.81	4.01	13.6	100	3.03	11.2	2.14	6.17
Melanoma												
LOX IMVI	5.41	100	3.45	100	1.75	3.39	10.6	28.9	1.68	3.36	1.86	3.78
MALME-3M	3.41	31.2	2.34	6.47	2.03	5.4	11.5	31.7	1.98	4.86	1.87	5.17
M14	5.17	100	5.24	23.7	2.1	5.49	9.82	34.1	2.17	5.53	2.09	5.66
MDA-MB-435	10.2	100	4.03	21.4	3.07	9.43	13.4	37.2	2.1	4.86	2.79	10.5
SK-MEL-2			10.1	23.6			13.9	30.1	1.72	3.26		
SK-MEL-28	17	100	6.79	26.3	3.11	11.7	17.8	74.8	2.68	8.7	3	12.2
SK-MEL-5	7.69	20.6	3.29	10.8	1.73	3.18	12.4	26.3	1.92	3.79	1.74	3.16
UACC-257	19.2	100	13.3	62.6	3.05	11.7	22.7	93.3	2.72	8	3.6	14.1
UACC-62	10.6	70.4	2.61	13.3	1.91	4.09	12.6	29.1	1.87	5.57	1.99	4.16
Ovarian cancer												
IGROV1	10.1	100	2.71	15.4	3.01	12.3	16	68	1.92	6.49	3.02	12.8
OVCAR-3	6.42	100	5.32	34.3	3.54	19.3	9.27	80	2.19	5.07	3.65	16.8
OVCAR-4	4.16	100	4.02	25.6	2.97	35.2	4.96	86.4	2.51	8.38	3.07	27.8
OVCAR-5	12	100	7.58	26.9	2.98	11.6	11.2	50.8	2.16	5.22	2.94	12.8
OVCAR-8			12.5	100			20.9	100	3.23	12.5		
NCI/ADR-RES	9.2	100			2.46	8					2.46	8.44
SK-OV-3	16.4	100	14.2	69.1	1.81	5.63	18.1	98.6	3.03	10.2	2.65	7.59
Renal cancer												
786-0	14.2	100	7.85	28.1	2.6	100	11.2	100	2.57	7.55	2.45	6.91
A498	100	100	15.1	45.2	3.07	39.7	33.3	100	3.1	8.71	2.46	7.86
ACHN	8.68	100	3.26	14.3	2.92	100	13.6	100	2.85	9.97	2.76	12.3
CAKI-1	5.83	100	4.01	24.2	2.8	100	7.91	32.9	2	7.2	3.04	12.9
RXF393	4.02	35.8	6.93	28.4	1.84	8.3	11.5	79.3	2.64	9.54	1.82	3.91
SN12C	8.52	100	3.3	15.8	2.17	38.3	12	100	2.59	8.35	2.23	11.4
TK-10	58.3	100	19.7	58.3	4.7	100	38	100	3.99	15.6	4.44	18.8
UO-31	2.69	100	2.07	14.9	2.26	100	2.38	72.7	2.09	8.61	2.55	12.8
Prostate cancer												
PC-3	2.85	100	1.95	12.4	2.5	100	3.19	100	2.25	9.31	2.54	11.9
DU-145	13.9	100	5.45	100	3.85	100	21	100	3.6	15.9	3.53	15.5
Breast cancer												
MCF7	3.09	100	3.13	24	1.89	100	6	100	2.43	10.8	2.11	6.27
MDA-MB-231	10	100	5.37	19.3	1.92	27.8	12.8	35.1	2.12	4.64	2.6	8.6
HS 578T	10.7	100	10.2	49.1	2.57	100	11.1	89.6	2.23	7.18	2.41	7.8
BT-549	3.93	30.9	2.56	8.18	1.3	12.4	6.07	27.4	2.17	4.78	1.81	4.44
T-47D	2.85	49.5	3.39	93.9	1.77	100	3.42	77.8	2.53	8.38	2.08	6.28
MDA-MB-468	10.5	56.8	3.44	15.5	1.97	8.19	19.1	100	2.59	9.56	1.9	4.56

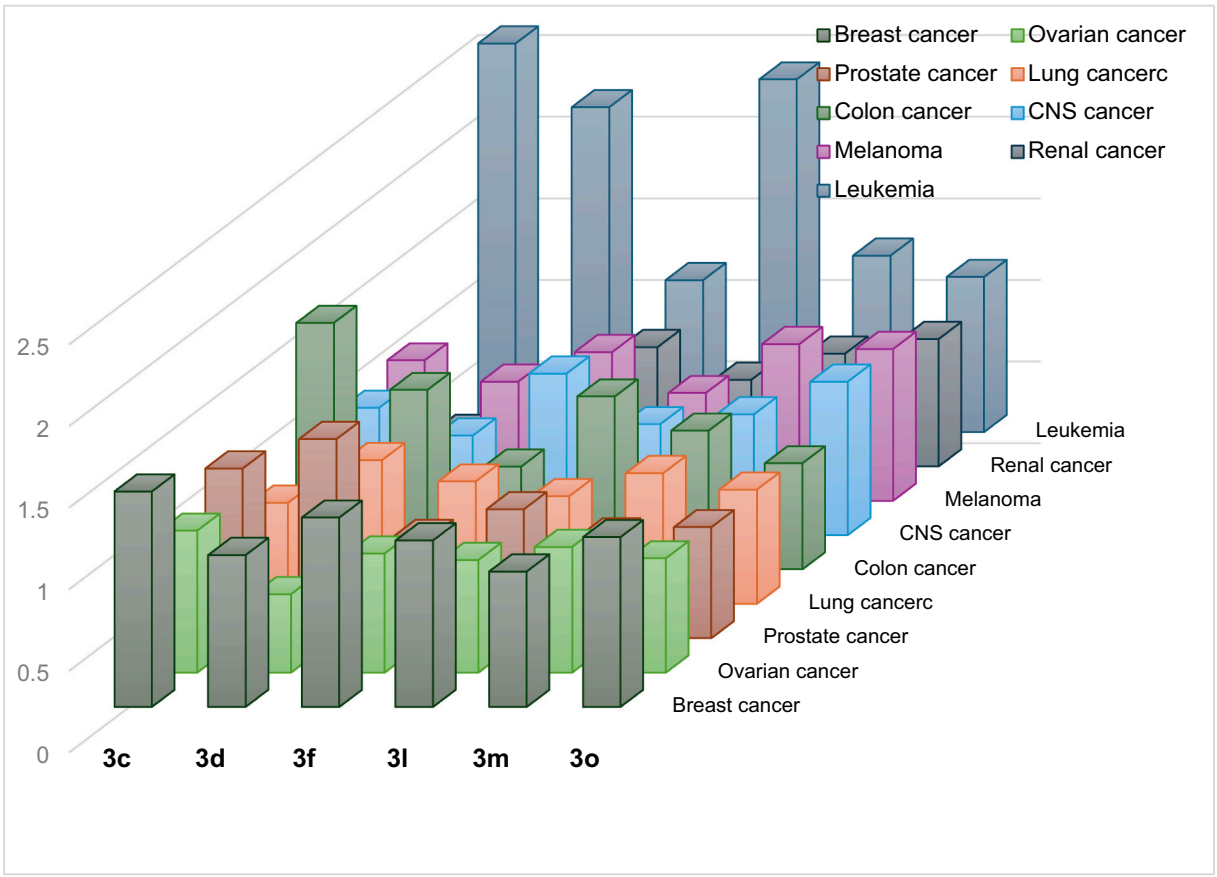

Fig. 6. The selectivity ratio of the test compounds towards 9 subpanels of NCI-60 human tumor cell lines.

potency when compared to lapatinib (IC_{50} of 44.49 nM), with respective IC_{50} values of 495.8, 326.3, 398.3, 392.8, and 323.3 nM. These findings show that HER2 kinase, which is abundantly expressed in BT474 BC cells, is a prominent target of the synthesized compounds **3r**, **3h**, **3n**, **3i**, and **3f**. These findings also suggest that HER2 kinase is a selective target of pyrazolo pyridine derivatives, in addition to other oncologic pathways that have been studied and discussed under the kinase target assay and apoptosis.

On the other hand, the mentioned compounds demonstrated strong antiproliferative activities against BT549 cells, as evidenced by their IC_{50} values ranging from 1024 to 76 nM. Among these, compounds **3b**, **3c**, **3h**, **3p**, **3n**, and **3f** demonstrated the highest potencies, with IC_{50} values of 299.1, 223.3, 112.4, 76.79, 189.1, and 282.6 nM, respectively. The best antiproliferative effect was remarked for compound **3p** (IC_{50} = 76.79 nM).

Moreover, the results of screening our compounds against ZR-75-30 cell line reviled that, most of these compounds have potent inhibition against ZR-75-30 with IC_{50} ranging from 241 to 909 nM. The strongest inhibition against ZR-75-30 cells was achieved by compound **3h** (IC_{50} 197.7 nM). Surprisingly, compounds **3m** and **3o** showed selective inhibition of ZR-75-30 cell lines (IC_{50} = 258.6 and 384.1 nM, respectively), compared to lower inhibitions of BT474 and BT549 (IC_{50} = 3773–584.7 nM) as shown in Table 3. Compound **3p**, however, showed selective inhibitions of BT549 cell lines (IC_{50} = 76.79 nM) in contrast to lesser inhibitions of ZR-75-30 and BT474 cells (IC50 = 1110 nM and 404.9 nM, respectively). Compounds **3h**, **3n**, and **3i** have strong antiproliferative activity against all BC cell lines, including BT474 (IC_{50} = 326.3, 398.3, and 392.8 nM), BT549 (IC50 = 112.4, 189.1, 360.1 nM), and ZR-75-30 (IC_{50} = 197.7, 361.4, and 403 nM), which is indicative of their potentially most potent multitarget anticancer actions.

2.2.7. Annexin V PI/FITC apoptosis assay using BT474 cell lines

we conducted an Annexin V Fluorescein Isothiocyanate/Propidium Iodide (FITC/PI) apoptosis assay for the most potent compounds namely **3f, 3o** and **3l** against BT474 cell lines at 0.5, 1, 5, and 10 μM concentrations. The selection of these compounds for the apoptosis assay was made considering their potent antiproliferative activities on triple-positive BT474 (with IC_{50} of 323.3, 642.8 and 5285 nM) (Table 2). (See Table 4.)

The results revealed both cells were resistant to apoptosis induction by all compounds. For example, compounds 3o and 3f induced a negligible level of early and late apoptosis against BT474 cells at 5 μM, of (8.1 % and 9.9 %) and (4.7 % and 3 %), compared to (9.8 % and 9 %) and (2.7 % and 2.9 %) of the control, respectively (Fig. 7). This is followed by compound **3l**, which exhibits mild late apoptosis at 0.5, 1 and 10 μM of (9.2 %, 9.4 % and 10.2 %) compared to 2.2 % of the control. In addition, compound 3o showed early and late apoptosis of 12.3 and 12.6 % respectively at 10 μM concentration. Moreover, the highest necrotic level can be seen with compounds 3i and 3f at 10 μM of (12.8 % and 10.5 %) compared to the control of (5.4 and 3.4 %), respectively.

Despite some degree of consistency with the antiproliferative assays, these results demonstrate the target specificity of our most potent compounds towards HER2 + ve harboring cells.

2.2.8. In vivo antitumor activity of compound 3f

Evaluation of antitumor effect of **3f** using xenograft mouse model.

The BC xenograft mouse model demonstrates that mice treated with compound **3f** and Lapatinib had lower bioluminescence intensities compared to vehicle controls (Fig. 8A–B). The recorded tumor size over the course of study showed a significant inhibition in tumor size by 19.45 % when mice treated with **3f**. On the other hand, mice treated with lapatinib exhibited a further decrease in tumor size by 38.6 %

Table 2
The selectivity ratio of compounds **3c**, **3m**, 3d, **3l**, 3o, and 3f, against NCI-60 human tumor cell lines.

Cancer	**3c**		**3d**		**3f**		**3l**		**3m**		**3o**	
Type	MID[a]	S[b]	MID	S	MID	S	MID	S	MID	S	MID	S
Leukemia	4.02	**2.6**	2.41	**2.2**	2.3	**1.1**	5.05	**2.4**	1.9	**1.3**	2.32	**1.2**
Lung	12.7	0.8	4.87	**1.1**	2.72	1	13.9	0.9	2.43	1	2.96	0.9
Colon	6.06	**1.7**	4.07	**1.3**	3.11	0.8	9.43	**1.3**	2.31	**1.1**	3.12	0.9
CNS	10.6	1	6.54	0.8	2.18	**1.2**	13.6	0.9	2.59	0.9	2.34	**1.1**
Melanoma	9.84	**1.1**	5.68	0.9	2.34	**1.1**	13.9	0.9	2.09	**1.2**	2.37	**1.1**
Ovarian	9.71	**1.1**	7.72	0.7	2.8	**0.9**	13.4	0.9	2.51	1	2.97	0.9
Renal	25.3	0.4	7.78	0.7	2.8	**0.9**	16.2	0.7	2.73	0.9	2.72	1
Prostate	8.38	**1.2**	3.7	**1.4**	3.18	0.8	12.1	1	2.93	0.8	3.04	0.9
Breast	6.85	**1.5**	4.68	**1.1**	1.9	**1.4**	9.75	**1.2**	2.35	**1**	2.15	**1.2**
MID-all[c]	10.4		5.27		2.59		11.9		2.43		2.66	

[a] Average GI_{50} of compound against cell lines of a particular subpanel in μM.
[b] Selectivity ratio obtained by dividing average GI_{50} of a compound against the full panel of NCI 60 cell lines by average GI_{50} of the same compound against a particular subpanel of cancer cell lines MID-all/MID i.e. Higher value indicates better selectivity.
[c] Average GI_{50} of a compound against the full panel of NCI 60 cell lines in μM.

Table 3
Protein kinase profiling of compounds **3o** and **3f** against a panel of 20 kinases, represented by % inhibitions and activations, in comparison with lapatinib and sorafenib as reference compounds using ADP-Glo Assay Method.

Kinase	**3f**	**3o**	Tucatinib
BRAF	5	3	−9
BTK	0	0	**−40**
CDK1/CyclinA1	0	−1	−12
CDK12	−6	1	−16
EGFR (ErbB1)	−16	−8	**−91**
ERK1	14	14	−9
FGFR1 (FLT2)	15	18	−13
FLT1	18	19	−12
FLT3	−18	−6	−17
HER2 (ErbB2)	**−88**	**−75**	**−90**
HER4 (ErbB4)	1	6	**−86**
JAK2	−4	12	4
KDR −8	2	1	−10
KIT	−16	−18	−10
MAPKAPK2	2	3	−3
MER	2	3	−9
MET	−2	−4	**−53**
p38 alpha	1	3	2
PDGFR-α	−8	−9	−15
SRC	2	0	−4

(−) values: inhibition of target activity.
(+) values: activation of target activity.
>−25 % changes in activity compared to control was considered.
To be significant inhibition and denoted in bold.

Table 4
IC_{50} Determinations for compounds **3o**, and **3f** tested against HER2 Kinase using ADP-Glo Method.

Best-fit-values	**3f**	**3o**
Log IC_{50}	2.333	2.3
R^2	0.9693	0.9579
No. of points analyzed	10	10
Standard error	0.04552	0.05595
IC_{50} (μM)	215	199

compared to the vehicle control mice (Fig. 8C–D). When BC xenografts were resected and weighed at the end of the experiment, there was a reduction ($p = 0.041$) in tumor weight in **3f**-treated mice and this reduction was increased in Lapatinib-treated compared to control mice (Fig. 8E). The mean body weight of control and treated mice did not show any significant differences over the course of the experiment (Fig. 8F). These results suggest that the compound **3f** is promising and exerted anti-tumor activity in in vivo BC model. In addition, it is relatively safe and comparable agent with Lapatinib because it did not change the total body weight in treated mice. In a previous study, compound **34e** (TAK-285) exerted a significant inhibition in BT-474 BC growth in the brain compared to mice received Lapatinib. [57] In our previous study, although other compounds showed a promise in BC cell culture, compound **17d** in that study was most effective and metabolically stable in preclinical model. [58] Ziegler et al. developed new class of compounds that can suppress the forkhead box M1 (FOXM1) and a few of them decreases tumor size in BC mice model and had very good pharmacokinetic profiles. [59] Thus, further studies are needed to evaluate its pharmacokinetic properties and to determine the highest tolerable dose.

Table 5
Antiproliferative activity (IC_{50}; nM) of compounds **3a–r** against HER2-expressing ductal BC cell lines.

Compound	BT-474 (IC_{50} ± SD) nM	BT-549 (IC_{50} ± SD) nM	ZR-75-30 (IC_{50} ± SD) nM
3a	3133 ± 70	400.3 ± 60	481.7 ± 72.3
3b	2103 ± 25	299.1 ± 44.9	241.4 ± 36.2
3c	1187 ± 78	223.3 ± 33.5	303.7 ± 45.6
3d	2717 ± 40	326.7 ± 49	308.1 ± 46.2
3e	4592 ± 38	968.7 ± 145.3	909.2 ± 13.4
3f	323.3 ± 48.5	282.6 ± 42.4	271.7 ± 40.8
3g	10,503 ± 75	416.1 ± 62.4	499.2 ± 74.9
3h	326.3 ± 49	112.4 ± 16.9	197.7 ± 29.7
3i	392.8 ± 59	360.1 ± 54	403 ± 60.5
3j	565.3 ± 84.8	1024 ± 53.6	540.7 ± 81.1
3k	1111 ± 67	221.8 ± 33.3	398.8 ± 59.8
3l	5285 ± 93	467.4 ± 20.1	418.8 ± 62.8
3m	3773 ± 66	584.7 ± 27.7	258.6 ± 38.8
3n	398.3 ± 59.7	189.1 ± 28.4	361.4 ± 54.2
3o	642.8 ± 96.4	601.5 ± 30.2	384.1 ± 57.6
3p	1110 ± 16.5	76.79 ± 11.5	404.9 ± 60.7
3q	1882 ± 82.3	470.1 ± 70.5	539.1 ± 80.9
3r	495.8 ± 74.4	312.6 ± 46.9	756.6 ± 13.5
Lapatinib	60.01 ± 11.7	2160 ± 13	420 ± 7

2.3. Molecular modeling

2.3.1. Docking studies

Docking studies are used to investigate potential binding modes of test compounds against target protein, HER2. Before docking, validation is required to confirm the validity of the docking software. This is done by redocking of the co-crystalized and comparing the docked pose with the co-crystalized pose. Fig. 9A, shows an overlapping of both poses where the software was able to predict the correct pose. Important interactions shown in Fig. 9B are maintained in the docking pose and includes hydrogen bonding with M801, halogen bond with L769 and several hydrophobic interactions with residues in the active site such as

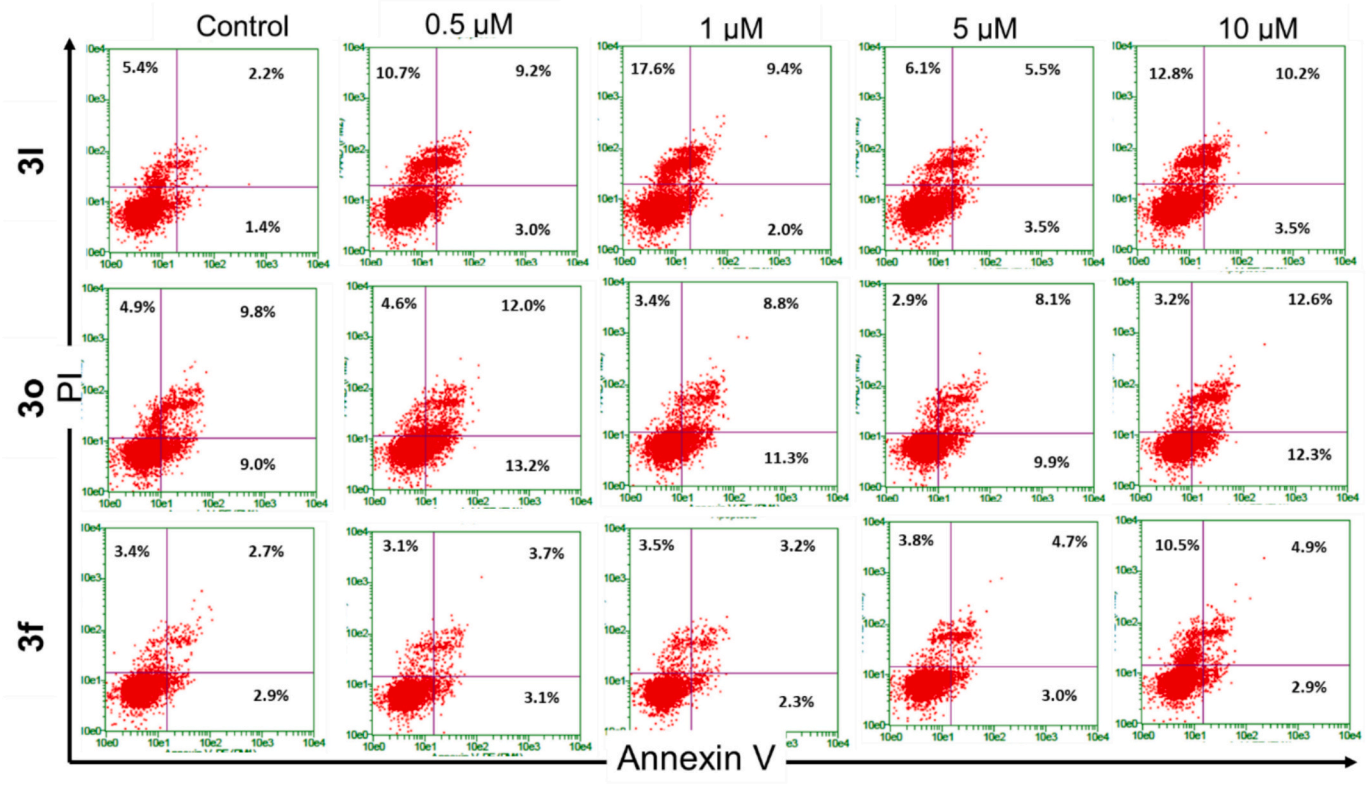

Fig. 7. Annexin V Fluorescein Isothiocyanate/Propidium Iodide (FITC/PI) apoptosis assay was performed on BT474 treated with compounds **3l**, **3o** and **3f** at 0.5, 1, 5, and 10 μM concentrations for a duration of 72 h. The X-axis represents annexin V, while the Y-axis represents PI. The quadrants are defined as follows: C1 (upper left): necrotic cells (PI+/annexin V-); C2 (upper right): late apoptotic cells (PI+/annexin V+); C3 (lower left): live cells (PI−/annexin V-); and C4 (lower right): early apoptotic cells (PI−/annexin V+). The presented data depicts the mean % cell number ± standard deviation (SD), based on three independent experiments ($n = 3$).

V734 and L852. Most of the tested compounds (**3a–r**) showed docked poses overlapped with the crystal structure pose. The docking pose of the most potent compounds 3o and 3f, are shown in Fig. 9C and D, respectively. Docking scores obtained from these docking studies are shown in Table 6. All compounds, showed docking scores comparable or better than the co-crystalized ligand, TAK-285, which showed a docking score of −9.7 kcal/mol. Among tested compounds, **3o** and **3f** showed the best docking scores of −10.7 and 10.9 kcal/mol, respectively. It worth to mention here that these two compounds are the most potent compounds in the enzyme inhibition studies. Docking studies are generally considered a static simulation of ligand -protein interaction which not necessarily demonstrate the full picture of interaction. In order to have a better understanding of this interaction especially in a dynamic manner considering time factor, molecular dynamic studies are generally required. Base in that, we decided to follow up on the docking studies using molecular dynamics (MD) with a special focus on 2 ligands **3o** and **3f** which showed the best results in both the biological and docking studies.

2.3.2. *Molecular dynamics studies*

Molecular dynamic simulation is used to study the stability of the formed complexes with the course of time. In this study, we used the HER2 kinase domain obtained from PDB 3RCD. Missing protein residues in the PDB file were constructed so that we have the full protein chain. This was done with the help of SWISS-model software [60]. After the construction of the full protein, four different systems were built and studied. These including the apoprotein, protein in complex with the co-crystalized pyrrolo[3,2-*d*]pyrimidin ligand (TAK-285) as obtained form the 3RCD PDB, protein in complex with 3o and in complex with **3f**. All runs were performed for 100 ns and the resulted trajectories were analyzed. For example, the root mean square deviation (RMSD) of the protein structure was stable in all the complexes as seen in Fig. 10A. The standard deviation of RMSD values for all the complexes are less than 0.5 Å (Table 7) which indicate the stability of the systems built. In addition, Radius of Gyration (R_g) (Fig. 10B) which is a measurement of the system compactness also showed good stability (standard deviation <0.2 Å) which further support the stability of the systems built. Furthermore, root mean square fluctuation (RMSF) of protein residues (Fig. 10C) was not affected by insertion of different ligand. Evaluation of ligand stability could be investigated by studying RMSD of ligand (Fig. 10D) and the hydrogen bonds between the ligand and protein (Fig. 10E). Compared to the co-crystalized ligand, TAK-285, which is a 17 nM inhibitor of HER2, **3o** showed comparable ligand RMSD of 2.4 ± 0.5 Å for **3o** compared to 2.3 ± 0.4 Å for TAK-285. Compound **3f** on the other hand, showed slightly increased ligand RMSD of 6.7 ± 1.6 Å. This suggests that **3o** and **3f** showed good interaction comparable to the co-crystalized ligand. Hydrogen bonds number is also a very important parameter in determining the stability of complexes. The number of hydrogen bonds for **3o** has been stable during the full 100 ns production run suggesting the stability of its complex with HER2. **3f** also showed stable hydrogen bonds that increased at the second half of the production run and stayed stable after that as seen in Fig. 8E. These results support the efficacy of these two compounds as demonstrated by the biological data.

3. Conclusion

In this study, we introduced a novel green one-pot synthesis for 18 pyrazolopyridine derivatives, several of which exhibited promising anticancer activity, particularly against HER2-positive breast cancer. Among them, compound 3f stood out for its strong in vitro and in vivo efficacy, including selective HER2 kinase inhibition and significant tumor suppression in a breast cancer xenograft model. Beyond reiterating these encouraging outcomes, this work highlights the potential of

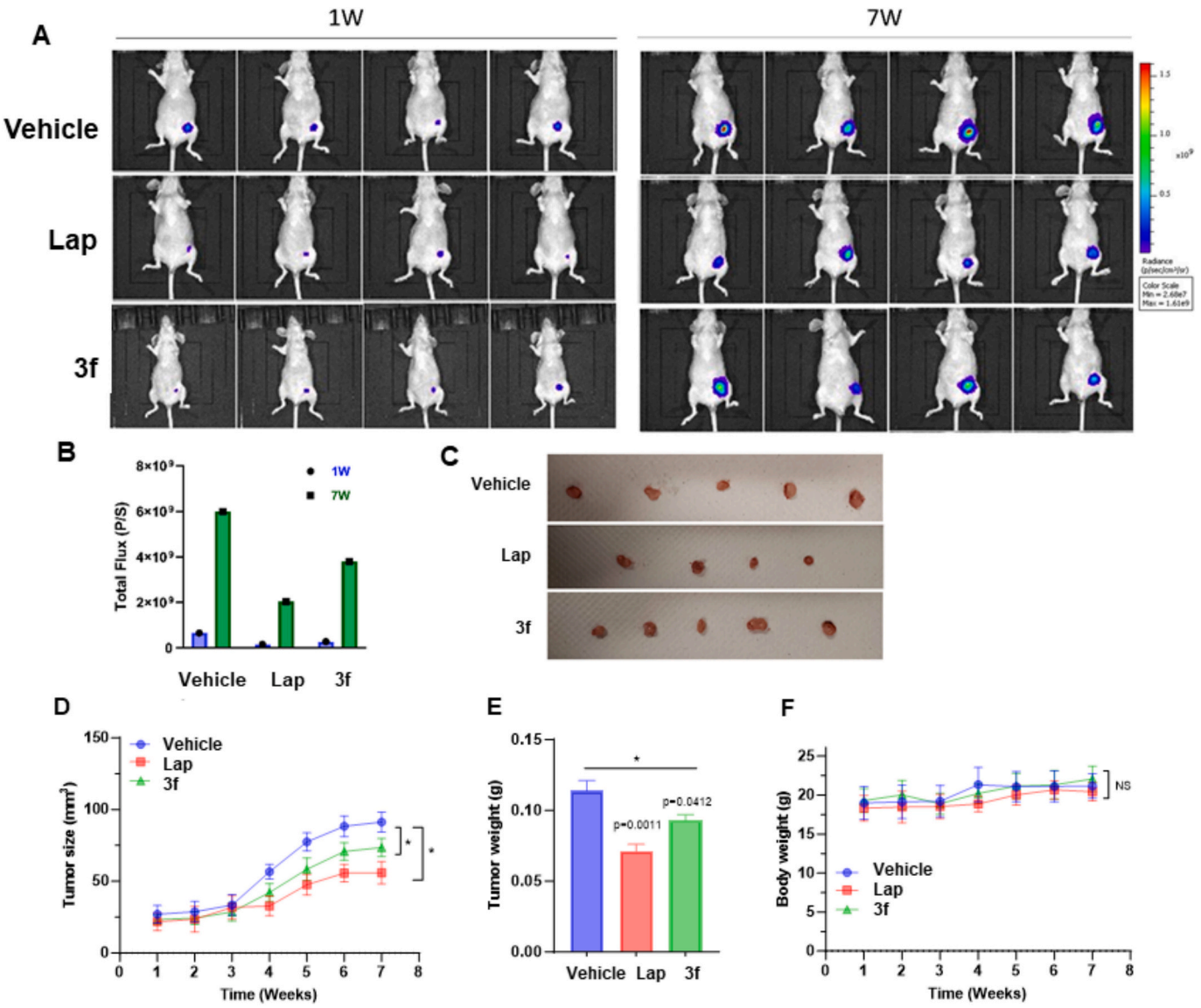

Fig. 8. Effect of antitumor activity of **3f** on breast cancer xenograft mice. **A:** Live imaging of BC xenograft by bioluminescence. The least intensity represented by blue colour while high intensity represented by red, **B**: Quantification of tumor luminescence, **C:** Representation of resected tumors from mice treated with **3f** in addition to mice received Lapatinib and vehicle control groups, **D**: Tumor size as recorded over the course of treatment, E: Tumor weight measured in grams, and **F**: Total body weight measured in grams. * Depicts significance at *p*-value of less than 0.05 corresponding to vehicle control mice. (For interpretation of the references to colour in this figure legend, the reader is referred to the web version of this article.)

pyrazolopyridine-based scaffolds as a platform for the development of selective kinase inhibitors. The selectivity of **3f** and **3o** towards HER2, as evidenced by kinase profiling and molecular docking, suggests a favorable therapeutic index, especially when compared to non-selective tyrosine kinase inhibitors like lapatinib.

Future research should focus on optimizing the pharmacological profiles of these derivatives, assessing their bioavailability, and exploring structure-activity relationships (SAR) to fine-tune HER2 specificity. In addition, broader in vivo efficacy studies across various HER2-expressing tumor types and investigations into resistance mechanisms will be essential to fully realize the therapeutic potential of this scaffold.

In conclusion, the findings offer a compelling foundation for continued development of pyrazolopyridine derivatives as targeted therapies in HER2-driven malignancies, paving the way towards more effective and safer treatment options for aggressive breast cancer subtypes.

4. Experimental

4.1. Chemistry

4.1.1. General

All chemicals and solvents were purchased from Sigma-Aldrich (USA) or Alfa-Aesar Organics and were used without further purification. Melting points were measured on a Stuart Scientific apparatus by using open capillary tube method. ^{1}H NMR spectra were recorded on a Bruker Ascend 400 MHz spectrometer and ^{13}C NMR spectra were recorded at 100 MHz in deuterated (DMSO-d_6). Chemical shift values (δ) are expressed as parts per million (ppm). All coupling constant (J) values were given in hertz (Hz). TLC was performed using silica gel plates to monitor the progression of reactions and check the purity of the products, using chloroform: methanol 9: 1 as the eluting system. Elemental analyses performed on a Thermo Scientific Flash 2000 elemental Analyzer and mass spectrometry recorded on a Thermo Scientific GCMS model ISQ mass spectrometer were carried out at the Regional Center for

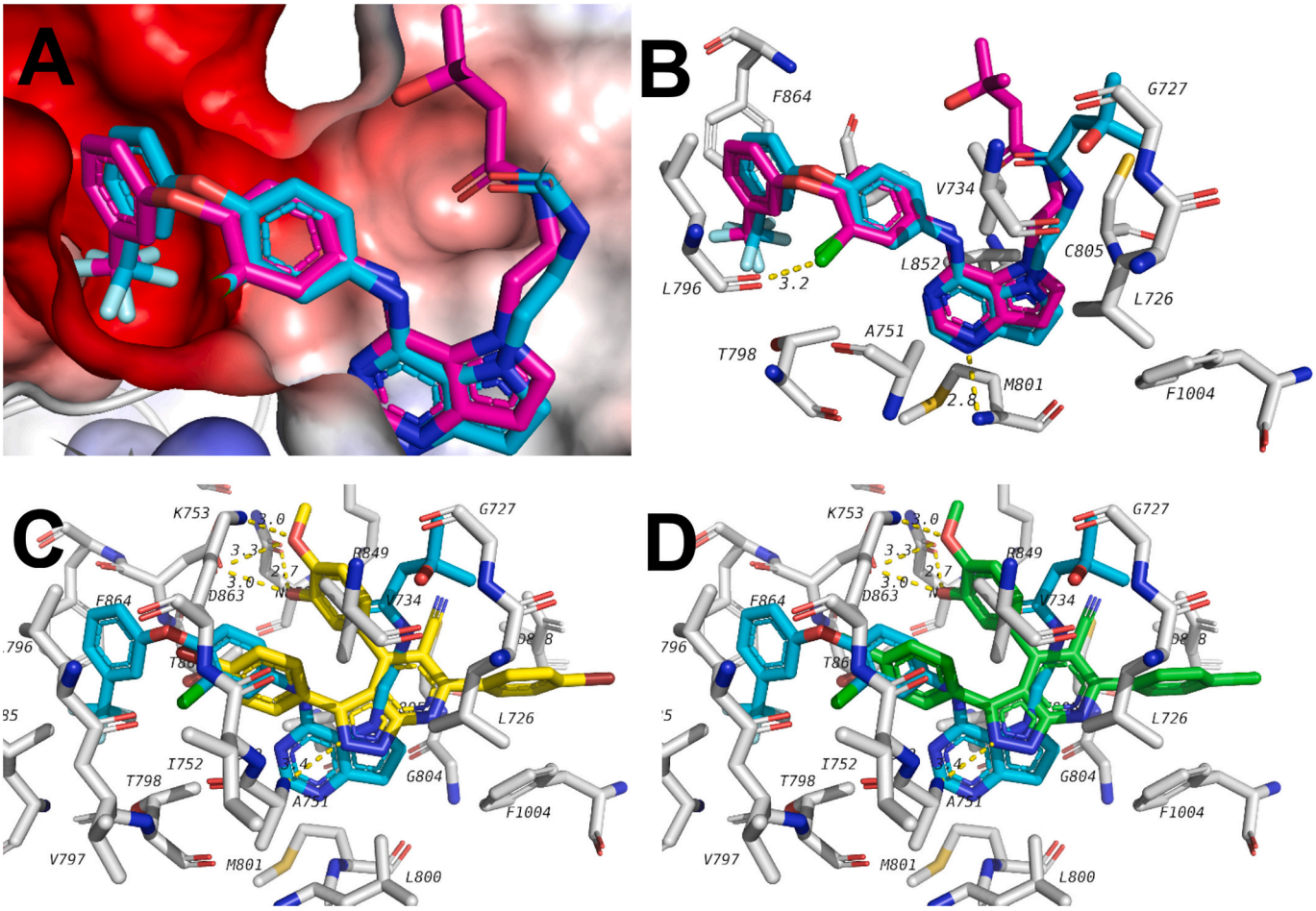

Fig. 9. Docking results of compounds against HER2 (PDB ID 3RCD). A. Overlapping of Docked pose (pink) and crystal pose (blue) for validation purpose. B. Interactions of co-crystalized ligand with the active site of HER2. C. Interactions of **3f** (yellow) with the active site. D. Interactions of **3o** (green) with the active site. (For interpretation of the references to colour in this figure legend, the reader is referred to the web version of this article.)

Table 6
Docking results of target compounds against HER2 (PDB ID: 3RCD).

Ligand	Docking score (kcal/Mol)
3a	−10.3
3b	−10.5
3c	−10.3
3d	−10.2
3e	−10.5
3f	−10.9
3g	−10.4
3h	−10.2
3i	−10.1
3j	−10.3
3k	−10.5
3l	−10.4
3m	−10.6
3n	−10.4
3o	−10.7
3p	−10.2
3q	−9.9
3r	−10.1
TAK-282	−9.7

Mycology and Biotechnology, Al-Azhar University, Cairo, Egypt. Mass spectral data were given as *m/z* (relative abundance %). The starting compounds **1a–b** and **2a–i** were prepared according to the previously reported methods. [56,61,62]

*4.1.2. General procedure for the synthesis of compounds **3a–r***

To a mixture of (4-sustituted phenyl)-3-oxopropanenitriles **1a or 1b** (0.0022 mol) and the aryl hydrazone derivatives **2a–i** (0.0013 mol) in ethanol (30 ml), 3 M HCl (150 μL) was added. The reaction mixture was refluxed for 72 h, cooled to room temperature, and quenched with water. The precipitate formed was filtered off and recrystallized from DMF/water mixture to afford the desired compounds **3a–r**.

*4.1.2.1. 3,6-Bis(4-bromophenyl)-4-phenyl-1H-pyrazolo[3,4-b]pyridine-5-carbonitrile (**3a**).* Yield: 399 mg, 58 %; m.p.: 282–283 C; ^{1}H NMR (DMSO-d_6, 400 MHz): δ 6.97 (d, 2H, Ar—Hs, J = 8.1 Hz), 7.28 (d, 2H, Ar—Hs, J = 8.1 Hz), 7.32–7.39 (m, 4H, Ar—Hs), 7.48 (t, 1H, Ar—H, J = 8.0 Hz), 7.84 (d, 2H, Ar—Hs, J = 8.0 Hz), 7.91 (d, 2H, Ar—Hs, J = 8.0 Hz), 14.67 (s, 1H, NH exchanged with D_2O); ^{13}C NMR (DMSO-d_6, 100 MHz): δ 100.90, 109.76, 117.69, 121.34, 123.83, 128.09, 129.33, 130.44, 130.61, 131.32, 131.43, 131.48, 133.84, 136.97, 145.08, 151.88, 158.83; Anal. Calcd for $C_{25}H_{14}Br_2N_4$ (530.22): C, 56.63; H, 2.66; N, 10.57. Found: C, 56.85; H, 2.89; N, 10.71; MS *m/z* (%): 530.17 (M^+, 40.65 %), 203.31 (100 %).

*4.1.2.2. 3,6-Bis(4-bromophenyl)-4-(4-fluorophenyl)-1H-pyrazolo[3,4-b]pyridine-5-carbonitrile (**3b**).* Yield: 442 mg, 62 %; m.p.: 319–321 C; ^{1}H NMR (DMSO-d_6, 400 MHz): δ 6.97 (d, 2H, Ar—Hs, J = 8.0 Hz), 7.18 (t, 2H, Ar—Hs, $^{3}J_{F\text{-}H}$ = 8.1 Hz), 7.35 (d, 2H, Ar—Hs, J = 8.0 Hz), 7.44 (t, 2H, Ar—Hs, $^{4}J_{F\text{-}H}$ = 8.1 Hz), 7.84 (d, 2H, Ar—Hs, J = 8.1 Hz), 7.91 (d, 2H, Ar—Hs, J = 8.1 Hz), 14.66 (s, 1H, NH exchanged with D_2O); ^{13}C NMR (DMSO-d_6, 100 MHz): δ 101.49, 110.44, 115.58 ($^{2}J_{F\text{-}C}$ = 22.0 Hz),

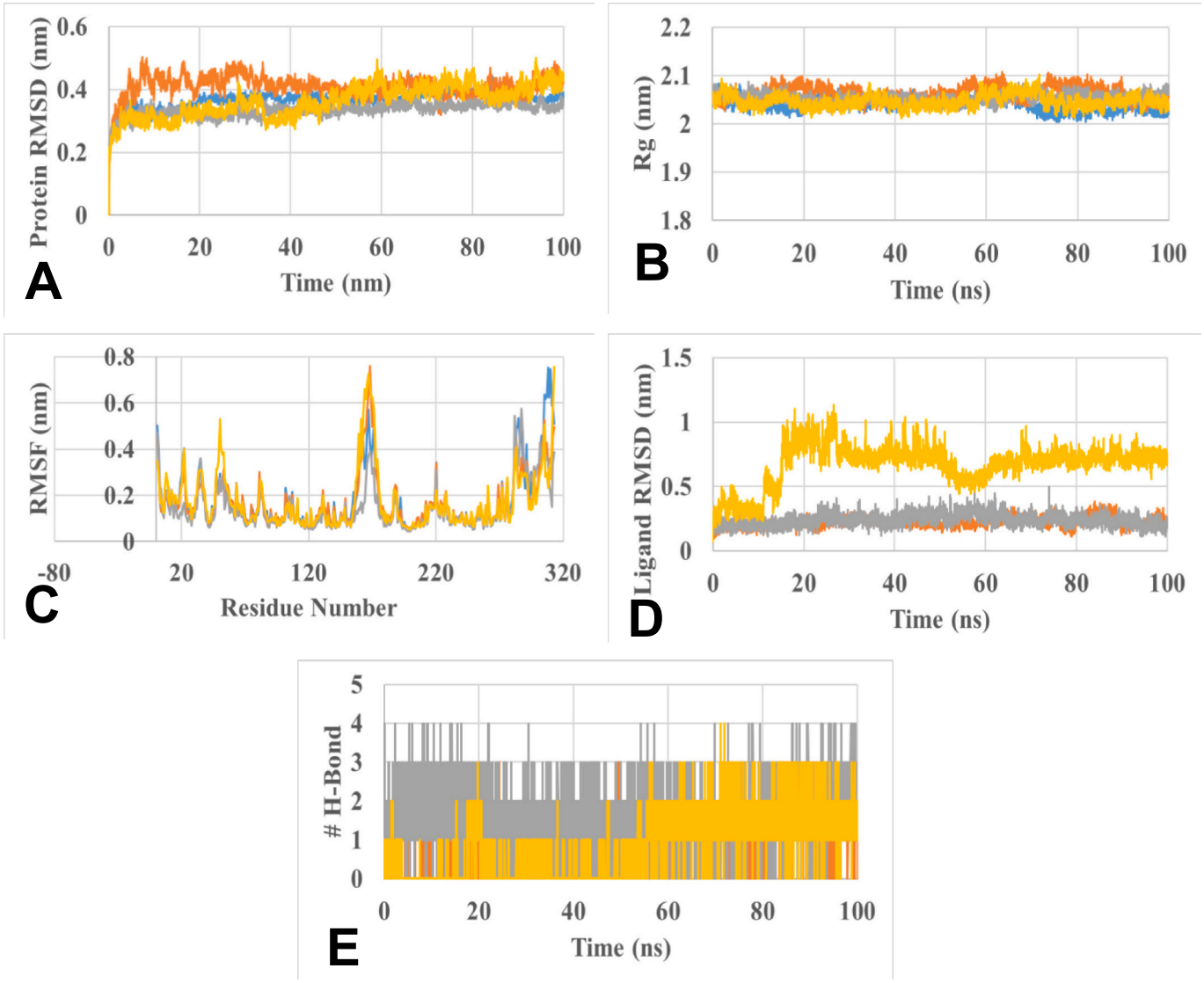

Fig. 10. Results of molecular dynamics studies. A, protein RMSD; B, Radius of gyration; C, RMSF of protein residues; D, ligand RMSD and E, number of hydrogen bonds. Blue is for apoprotein, orange for control, yellow for **3f** and grey for **3o.** (For interpretation of the references to colour in this figure legend, the reader is referred to the web version of this article.)

Table 7
Results of Molecular dynamics studies.

	Apoprotein	Control	3f	3o
RMSD of protein (nm)	0.313 ± 0.029	0.380 ± 0.034	0.292 ± 0.050	0.302 ± 0.021
Rg (nm)	2.041 ± 0.013	2.063 ± 0.014	2.047 ± 0.013	2.053 ± 0.009
RMSF (nm)	0.177 ± 0.130	0.172 ± 0.114	0.176 ± 0.129	0.147 ± 0.099
RMSD of ligand (nm)	–	0.225 ± 0.039	0.673 ± 0.159	0.239 ± 0.046
Number of H-bonds	–	1.150 ± 0.470	0.795 ± 0.802	1.647 ± 0.765

118.11 (C≡N), 121.95, 124.36, 130.64, 130.97, 131.23, 131.87, 131.97, 132.23 ($^{3}J_{F\text{-}C}$ = 9.0 Hz), 137.38, 145.52 (C=N), 151.32, 152.68, 159.25, 162.15, 164.61; Anal. Calcd for $C_{25}H_{13}Br_2FN_4$ (548.21): C, 54.77; H, 2.39; N, 10.22. Found: C, 55.03; H, 2.50; N, 10.49; MS *m/z* (%): 548.59 (M^+, 21.81 %), 203.84 (100 %).

*4.1.2.3. 3,6-Bis(4-bromophenyl)-4-(3-methoxyphenyl)-1H-pyrazolo[3,4-b]pyridine-5-carbonitrile (**3c**).* Yield: 444 mg, 61 %; m.p.: 268–270 C; ^{1}H NMR (DMSO-d_6, 400 MHz): δ 3.55 (s, 3H, OCH_3), 6.82 (br. s, 1H, Ar—H), 6.96 (s, 1H, Ar—H), 6.98 (s, 1H, Ar—H), 7.01–7.06 (m, 2H, Ar—Hs), 7.29–7.34 (m, 3H, Ar—Hs), 7.83 (d, 2H, Ar—Hs, *J* = 8.1 Hz), 7.90 (d, 2H, Ar—Hs, *J* = 8.1 Hz), 14.64 (s, 1H, NH exchanged with D_2O); ^{13}C NMR (DMSO-d_6, 100 MHz): δ 55.55 ($O\underline{C}H_3$), 101.17, 110.16, 115.63, 116.14, 118.19 (C≡N), 121.87, 122.04, 124.32, 129.95, 130.86, 131.06, 131.91, 131.94, 135.31, 137.44, 145.55 (C=N), 152.05, 152.71, 159.32, 162.79; Anal. Calcd for $C_{26}H_{16}Br_2N_4O$ (560.25): C, 55.74; H, 2.88; N, 10.00. Found: C, 55.87; H, 3.04; N, 10.26; MS *m/z* (%): 560.05 (M^+, 29.81 %), 487.58 (100 %).

*4.1.2.4. 3,6-Bis(4-bromophenyl)-4-(4-(trifluoromethyl)phenyl)-1H-pyrazolo[3,4-b]pyridine-5-carbonitrile (**3d**).* Yield: 606 mg, 78 %; m.p.: 288–289 C; ^{1}H NMR (DMSO-d_6, 400 MHz): δ 6.92 (d, 2H, Ar—Hs, *J* = 8.0 Hz), 7.25 (d, 2H, Ar—Hs, *J* = 8.1 Hz), 7.58 (d, 2H, Ar—Hs, *J* = 8.0 Hz), 7.66 (d, 2H, Ar—Hs, *J* = 8.1 Hz), 7.85 (d, 2H, Ar—Hs, *J* = 8.0 Hz), 7.92 (d, 2H, Ar—Hs, *J* = 8.0 Hz), 14.70 (s, 1H, NH exchanged with D_2O); ^{13}C NMR (DMSO-d_6, 100 MHz): δ 101.02, 110.51, 117.89 (C≡N), 122.01, 123.03, 124.47, 125.36, 125,39, 130.75, 130.92, 131.15,

131.46, 131.88, 132.04, 137.26, 138.13, 145.49 (C═N), 150.69, 152.58, 159.20; Anal. Calcd for $C_{26}H_{13}Br_2F_3N_4$ (598.22): C, 52.20; H, 2.19; N, 9.37. Found: C, 52.43; H, 2.40; N, 9.59; MS *m/z* (%): 598.79 (M^+, 17.98 %), 480.83 (100 %).

*4.1.2.5. 3,6-Bis(4-bromophenyl)-4-(3,4-dimethoxyphenyl)-1H-pyrazolo [3,4-b]pyridine-5-carbonitrile (**3e**).* Yield: 476 mg, 62 %; m.p.: 274–276 ℃; ^{1}H NMR (DMSO-d_6, 400 MHz): δ 3.40 (s, 3H, OCH_3), 3.82 (s, 3H, OCH_3), 6.82 (s, 1H, Ar—H), 6.97–7.08 (m, 4H, Ar—Hs), 7.33 (d, 2H, Ar—Hs, J = 8.2 Hz), 7.83 (d, 2H, Ar—Hs, J = 8.3 Hz), 7.90 (d, 2H, Ar—Hs, J = 8.4 Hz), 14.59 (s, 1H, NH exchanged with D_2O); ^{13}C NMR (DMSO-d_6, 100 MHz): δ 55.72 ($O\underline{C}H_3$), 56.30 ($O\underline{C}H_3$), 101.16, 110.23, 112.02, 114.36, 118.52 (C≡N), 121.84, 122.92, 124.25, 126.32, 130.83, 131.21, 131.90, 137.54, 145.63 (C═N), 148.73, 150.68, 152.21, 152.75, 159.45; Anal. Calcd for $C_{27}H_{18}Br_2N_4O_2$ (590.28): C, 54.94; H, 3.07; N, 9.49; O. Found: C, 55.16; H, 3.29; N, 9.71; MS *m/z* (%): 590.32 (M^+, 11.05 %), 481.28 (100 %).

*4.1.2.6. 3,6-Bis(4-bromophenyl)-4-(3-hydroxy-4-methoxyphenyl)-1H-pyrazolo[3,4-b]pyridine-5-carbonitrile (**3f**).* Yield: 539 mg, 75 %; m.p.: 308–310 C; ^{1}H NMR (DMSO-d_6, 400 MHz): δ 3.80 (s, 3H, OCH_3), 6.64 (dd, 1H, Ar—H, J = 2.08 Hz and 8.2 Hz), 6.78 (d, 1H, Ar—H, J = 8.4 Hz), 6.84 (d, 1H, Ar—H, J = 2.1 Hz), 7.00 (d, 2H, Ar—Hs, J = 8.4 Hz), 7.31 (d, 2H, Ar—Hs, J = 8.4 Hz), 7.82 (d, 2H, Ar—Hs, J = 8.6 Hz), 7.88 (d, 2H, Ar—Hs, J = 8.6 Hz), 9.19 (s, 1H, OH exchanged with D_2O),14.56 (s, 1H, NH exchanged with D_2O); ^{13}C NMR (DMSO-d_6, 100 MHz): δ 56.35 ($O\underline{C}H_3$), 101.14, 110.31, 112.19, 117.01, 118.39 (C≡N), 121.53, 121.77, 124.20, 126.72, 130.80, 131.03, 131.88, 131.90, 132.02, 137.55, 145.63 (C═N), 146.83, 149.49, 152.46, 152.72, 159.38; Anal. Calcd for $C_{26}H_{16}Br_2N_4O_2$ (576.25): C, 54.19; H, 2.80; N, 9.72. Found: C, 54.48; H, 2.96; N, 9.97; MS *m/z* (%): 576.78 (M^+, 13.99 %), 442.44 (100 %).

*4.1.2.7. 3,6-Bis(4-bromophenyl)-4-(4-ethoxy-3-methoxyphenyl)-1H-pyrazolo[3,4-b]pyridine-5-carbonitrile (**3g**).* Yield: 503 mg, 64 %; m.p.: 275–277 C; ^{1}H NMR (DMSO-d_6, 400 MHz): δ 1.37 (t, 3H. $CH_2\underline{CH_3}$, J = 6.9 Hz), 3.44 (s, 3H, OCH_3), 4.08 (q, 2H. $\underline{CH_2}CH_3$, J = 6.9 Hz), 6.85 (d, 1H, Ar—H, J = 1.8 Hz), 6.93 (d, 1H, Ar—H, J = 8.3 Hz), 6.98–7.01 (m, 3H, Ar—Hs), 7.32 (d, 2H, Ar—Hs, J = 8.4 Hz), 7.82 (d, 2H, Ar—Hs, J = 8.5 Hz), 7.90 (d, 2H, Ar—Hs, J = 8.5 Hz),14.58 (s, 1H, NH exchanged with D_2O); ^{13}C NMR (DMSO-d_6, 100 MHz): δ 15.05 ($OCH_2\underline{C}H_3$), 55.72 ($O\underline{C}H_3$), 64.53 ($OCH_2\underline{C}H_3$), 101.12, 110.23, 113.10, 114.37, 118.51 (C≡N), 121.84, 122.92, 124.23, 126.24, 130.84, 131.20, 131.89, 137.51, 145.69(C═N), 148.92, 149.72, 152.29, 159.50; Anal. Calcd for $C_{28}H_{20}Br_2N_4O_2$ (604.30): C, 55.65; H, 3.34; N, 9.27. Found: C, 55.47; H, 3.51; N, 9.52; MS *m/z* (%): 604.71 (M^+, 20.76 %), 387.92 (100 %).

*4.1.2.8. 3,6-Bis(4-bromophenyl)-4-(3,4,5-trimethoxyphenyl)-1H-pyrazolo [3,4-b]pyridine-5-carbonitrile (**3h**).* Yield: 508 mg, 63 %; m.p.: 266–268 ℃; ^{1}H NMR (DMSO-d_6, 400 MHz): δ 3.55 (s, 6H, 2 OCH_3), 3.72 (s, 3H, OCH_3), 6.69 (s, 2H, Ar—Hs), 7.01 (d, 2H, Ar—Hs, J = 8.4 Hz), 7.32 (d, 2H, Ar—Hs, J = 8.4 Hz), 7.83 (d, 2H, Ar—Hs, J = 8.6 Hz), 7.91 (d, 2H, Ar—Hs, J = 8.6 Hz),14.61 (s, 1H, NH exchanged with D_2O); ^{13}C NMR (DMSO-d_6, 100 MHz): δ 56.28 (2 $O\underline{C}H_3$). 60.71 ($O\underline{C}H_3$), 101.01, 108.12, 110.24, 118.34 (C≡N), 121.87, 124.30, 129.08, 130.81, 131.14, 131.89, 131.92, 137.44, 139.18, 145.69 (C═N), 152.15, 152.66, 153.04, 159.41; Anal. Calcd for $C_{28}H_{20}Br_2N_4O_3$ (620.30): C, 54.22; H, 3.25; N, 9.03. Found: C, 54.01; H, 3.54; N, 9.31; MS *m/z* (%): 620.96 (M^+, 32.75 %), 113.78 (100 %).

*4.1.2.9. 3,6-Bis(4-bromophenyl)-4-(thiophen-2-yl)-1H-pyrazolo[3,4-b] pyridine-5-carbonitrile (**3i**).* Yield: 488 mg, 70 %; m.p.: 272–274 C; ^{1}H NMR (DMSO-d_6, 400 MHz): δ 7.08–7.11 (m, 3H, Ar—Hs), 7.29 (dd, 1H, Ar—H, J = 1.1 Hz and 3.6 Hz), 7.38 (d, 2H, Ar—Hs, J = 8.4 Hz), 7.77–7.82 (m, 3H, Ar—Hs), 7.88 (d, 2H, Ar—Hs, J = 8.6 Hz), 14.69 (s, 1H, NH exchanged with D_2O); ^{13}C NMR (DMSO-d_6, 100 MHz): δ 102.10, 110.50, 118.06 (C≡N), 122.00, 124.36, 127.90, 130.57, 131.12, 131.88, 131.91, 133.57, 137.24, 145.06, 145.47 (C═N), 152.68, 159.45; Anal. Calcd for $C_{23}H_{12}Br_2N_4S$ (536.25): C, 51.52; H, 2.26; N, 10.45. Found: C, 51.75; H, 2.43; N, 10.71; MS *m/z* (%): 536.13 (M^+, 12.26 %), 168.73 (100 %).

*4.1.2.10. 3,6-Bis(4-chlorophenyl)-4-phenyl-1H-pyrazolo[3,4-b]pyridine-5-carbonitrile (**3j**).* Yield: 407 mg, 71 %; m.p.: 295–297 C; ^{1}H NMR (DMSO-d_6, 400 MHz): δ 7.02–7-05 (m, 2H, Ar—Hs), 7.14 (d, 2H, Ar—Hs, J = 8.1 Hz), 7.31–7.39 (m, 4H, Ar—Hs), 7.46 (m, 1H, Ar—H), 7.70 (d, 2H, Ar—Hs, J = 8.0 Hz), 7.98 (d, 2H, Ar—Hs, J = 8.0 Hz), 14.64 (s, 1H, NH exchanged with D_2O); ^{13}C NMR (DMSO-d_6, 100 MHz): δ 15.46101.14, 109.99, 117.90, 127.72, 128.29, 128.75, 129.54, 129.81, 130.55, 131.17, 131.42, 132.88, 134.04, 135.23, 136.82, 145.23, 152.07, 152.43, 158.96; Anal. Calcd for $C_{25}H_{14}Cl_2N_4$ (441.32): C, 68.04; H, 3.20; N, 12.70. Found: C, 68.29; H, 3.36; N, 12.89; MS *m/z* (%): 441.94 (M^+, 10.96 %), 48.00 (100 %).

*4.1.2.11. 3,6-Bis(4-chlorophenyl)-4-(4-fluorophenyl)-1H-pyrazolo[3,4-b] pyridine-5-carbonitrile (**3k**).* Yield: 442 mg, 74 %; m.p.: 322–324 C; ^{1}H NMR (DMSO-d_6, 400 MHz): δ 7.05 (d, 2H, Ar—Hs, J = 8.5 Hz), 7.15–7.22 (m, 4H, Ar—Hs), 7.43 (dd, 2H, Ar—Hs, $^4J_{F\text{-}H}$ = 5.4 Hz and 8.7 Hz), 7.69 (d, 2H, Ar—Hs, J = 8.5 Hz), 7.97 (d, 2H, Ar—Hs, J = 8.6 Hz), 14.63 (s, 1H, NH exchanged with D_2O); ^{13}C NMR (DMSO-d_6, 100 MHz): δ 15.46 (aliph-C), 108.65, 115.81, 120.56, 148.69, 152.21, 155.04; Anal. Calcd for $C_{25}H_{13}Cl_2FN_4$ (459.31): C, 65.38; H, 2.85; N, 12.20. Found: C, 65.12; H, 3.01; N, 12.42; MS *m/z* (%): 458.14 (M^+, 21.35 %), 46.71 (100 %).

*4.1.2.12. 3,6-Bis(4-chlorophenyl)-4-(3-methoxyphenyl)-1H-pyrazolo[3,4-b]pyridine-5-carbonitrile (**3l**).* Yield: 423 mg, 69 %; m.p.: 266–268 C; ^{1}H NMR (DMSO-d_6, 400 MHz): δ 3.55 (s, 3H, OCH_3), 6.83 (d, 1H, Ar—H, J = 1.5 Hz), 7.00–7.05 (m, 4H, Ar—Hs), 7.16 (d, 2H, Ar—Hs, J = 8.4 Hz), 7.30 (t, 1H, Ar—H, J = 7.9 Hz), 7.69 (d, 2H, Ar—Hs, J = 8.5 Hz), 7.97 (d, 2H, Ar—Hs, J = 8.5 Hz), 14.62 (s, 1H, NH exchanged with D_2O); ^{13}C NMR (DMSO-d_6, 100 MHz): δ 55.52 ($O\underline{C}H_3$), 101.19, 110.17, 115.56, 116.17, 118.18 (C≡N), 122.03, 127.29, 128.99, 129.91, 130.78, 131.68, 133.22, 135.31, 135.49, 137.08, 145.48 (C═N), 152.03, 152.68, 159.23, 159.31; Anal. Calcd for $C_{26}H_{16}Cl_2N_4O$ (471.34): C, 66.25; H, 3.42; N, 11.89. Found: C, 66.13; H, 3.56; N, 12.08; MS *m/z* (%): 471.26 (M^+, 20.11 %), 184.03 (100 %).

*4.1.2.13. 3,6-Bis(4-chlorophenyl)-4-(4-(trifluoromethyl)phenyl)-1H-pyrazolo[3,4-b]pyridine-5-carbonitrile (**3m**).* Yield: 497 mg, 75 %; m.p.: 255–257 C; ^{1}H NMR (DMSO-d_6, 400 MHz): δ 6.99 (d, 2H, Ar—Hs, J = 8.0 Hz), 7.11 (d, 2H, Ar—Hs, J = 8.0 Hz), 7.59 (d, 2H, Ar—Hs, J = 12.0 Hz), 7.66 (d, 2H, Ar—Hs, J = 8.1 Hz), 7.71 (d, 2H, Ar—Hs, J = 8.1 Hz), 7.99 (d, 2H, Ar—Hs, J = 8.0 Hz), 14.69 (s, 1H, NH exchanged with D_2O); ^{13}C NMR (DMSO-d_6, 100 MHz): δ 101.07, 110.53, 117.88 (C≡N), 123.03, 125.34, 125.38, 127.98, 129.10, 130.75, 130.90, 131.13, 131.65, 133.42, 135.65, 136.91, 138.16, 145.43 (C═N), 150.69, 152.58, 159.11; Anal. Calcd for $C_{26}H_{13}Cl_2F_3N_4$ (509.31): C, 61.32; H, 2.57; N, 11.00. Found: C, 61.50; H, 2.78; N, 11.23; MS *m/z* (%): 509.43 (M^+, 15.94 %), 436.21 (100 %).

*4.1.2.14. 3,6-Bis(4-chlorophenyl)-4-(3,4-dimethoxyphenyl)-1H-pyrazolo [3,4-b]pyridine-5-carbonitrile (**3n**).* Yield: 430 mg, 66 %; m.p.: 262–264 ℃; ^{1}H NMR (DMSO-d_6, 400 MHz): δ 3.39 (s, 3H, OCH_3), 3.82 (s, 3H, OCH_3), 6.81 (s, 1H, Ar—H), 7.00 (d, 1H, Ar—H, J = 8.1 Hz), 7.05–7.11 (m, 3H, Ar—Hs), 7.21 (d, 2H, Ar—Hs, J = 8.1 Hz), 7.70 (d, 2H, Ar—Hs, J = 8.0 Hz), 7.98 (d, 2H, Ar—Hs, J = 8.0 Hz), 14.59 (s, 1H, NH exchanged with D_2O); ^{13}C NMR (DMSO-d_6, 100 MHz): δ 55.68 ($O\underline{C}H_3$), 56.28 ($O\underline{C}H_3$), 101.23, 110.25, 112.00, 114.34, 118.55 (C≡N), 122.89, 126.32, 127.93, 129.00, 130.96, 131.70, 133.22, 135.45, 137.20,

145.59 (C═N), 148.69, 150.65, 152.21, 152.74, 159.41; Anal. Calcd for $C_{27}H_{18}Cl_2N_4O_2$ (501.37): C, 64.68; H, 3.62; N, 11.18. Found: C, 64.51; H, 3.80; N, 11.42; MS *m/z* (%): 501.59 (M^+, 22.43 %), 307.32 (100 %).

*4.1.2.15. 3,6-Bis(4-chlorophenyl)-4-(3-hydroxy-4-methoxyphenyl)-1H-pyrazolo[3,4-b]pyridine-5-carbonitrile (**3o**).* Yield: 405 mg, 64 %; m.p.: 300–302 C; ^{1}H NMR (DMSO-d_6, 400 MHz): δ 3.80 (s, 3H, OCH_3), 6.68 (dd, 1H, Ar—H, J = 2.1 Hz and 8.3 Hz), 6.79–6.82 (m, 2H, Ar—Hs), 7.07 (d, 2H, Ar—Hs, J = 8.5 Hz), 7.18 (d, 2H, Ar—Hs, J = 8.5 Hz), 7.68 (d, 2H, Ar—Hs, J = 8.5 Hz), 7.95 (d, 2H, Ar—Hs, J = 8.5 Hz), 9.18 (s, 1H, OH exchanged with D_2O), 14.55 (s, 1H, NH exchanged with D_2O); ^{13}C NMR (DMSO-d_6, 100 MHz):): δ 56.31 (OCH_3), 101.15, 110.30, 112.15, 117.01, 118.40 (C≡N), 121.49, 126.69, 127.87, 128.93, 130.75, 131.60, 131.66, 133.12, 135.41, 137.14, 145.59 (C═N), 146.77, 149.47, 152.45, 152.68, 159.33; Anal. Calcd for $C_{26}H_{16}Cl_2N_4O_2$ (487.34): C, 64.08; H, 3.31; N, 11.50. Found: C, 64.29; H, 3.38; N, 11.78; MS *m/z* (%): 487.87 (M^+, 37.62 %), 204.75 (100 %).

*4.1.2.16. 3,6-Bis(4-chlorophenyl)-4-(4-ethoxy-3-methoxyphenyl)-1H-pyrazolo[3,4-b]pyridine-5-carbonitrile (**3p**).* Yield: 449 mg, 67 %; m.p.: 249–251 C; ^{1}H NMR (DMSO-d_6, 400 MHz): δ 1.36 (t, 3H. CH_2CH_3, J = 6.0 Hz), 3.43 (s, 3H, OCH_3), 4.08 (q, 2H. CH_2CH_3, J = 8.1 Hz), 6.84 (d, 1H, Ar—H), 6.96 (d, 1H, Ar—H, J = 8.2 Hz), 7.02–7.08 (m, 3H, Ar—Hs), 7.20 (d, 2H, Ar—Hs, J = 8.2 Hz), 7.69 (d, 2H, Ar—Hs, J = 8.2 Hz), 7.97 (d, 2H, Ar—Hs, J = 8.3 Hz), 14.58 (s, 1H, NH exchanged with D_2O); ^{13}C NMR (DMSO-d_6, 100 MHz): δ 15.07 (OCH_2CH_3), 55.69 (OCH_3), 64.48 (OCH_2CH_3), 101.22, 110.25, 113.06, 114.41, 118.55 (C≡N), 122.89, 126.27, 127.95, 129.00, 130.95, 131.70, 133.21, 135.45, 137.20, 145.61 (C═N), 148.89, 149.74, 152.25, 152.74, 159.50; Anal. Calcd for $C_{28}H_{20}Cl_2N_4O_2$ (514.10): C, 65.25; H, 3.91; N, 10.87. Found: C, 65.03; H, 4.12; N, 11.09; MS *m/z* (%): 513.68 (M^+, 32.58 %), 315.58 (100 %).

*4.1.2.17. 3,6-Bis(4-chlorophenyl)-4-(3,4,5-trimethoxyphenyl)-1H-pyrazolo[3,4-b]pyridine-5-carbonitrile (**3q**).* Yield: 435 mg, 63 %; m.p.: 246–248 C; ^{1}H NMR (DMSO-d_6, 400 MHz): δ 3.55 (s, 6H, 2 OCH_3), 3.71 (s, 3H, OCH_3), 6.70 (br. s, 2H, Ar—Hs), 7.08 (d, 2H, Ar—Hs, J = 8.4 Hz), 7.24 (d, 2H, Ar—Hs, J = 8.3 Hz), 7.70 (d, 2H, Ar—Hs, J = 8.4 Hz), 7.98 (d, 2H, Ar—Hs, J = 8.4 Hz), 14.61 (s, 1H, NH exchanged with D_2O); ^{13}C NMR (DMSO-d_6, 100 MHz): δ 56.29 (2 OCH_3). 60.66 (OCH_3), 101.09, 108.16, 110.28, 118.34 (C≡N), 127.90, 129.00, 129.09, 130.87, 131.68, 131.92, 133.24, 135.50, 137.11, 139.21, 145.61 (C═N), 152.13, 152.65, 153.05, 159.28; Anal. Calcd for $C_{28}H_{20}Cl_2N_4O_3$ (531.39): C, 63.29; H, 3.79; N, 10.54. Found: C, 63.05; H, 3.98; N, 10.78; MS *m/z* (%): 531.34 (M^+, 38.43 %), 258.18 (100 %).

*4.1.2.18. 3,6-Bis(4-chlorophenyl)-4-(thiophen-2-yl)-1H-pyrazolo[3,4-b]pyridine-5-carbonitrile (**3r**).* Yield: 425 mg, 73 %; m.p.: 275–277 C; ^{1}H NMR (DMSO-d_6, 400 MHz): δ 7.11 (dd, 1H, Ar—H, J = 4.1 Hz and 4.1 Hz), 7.17 (d, 2H, Ar—Hs, J = 8.1 Hz), 7.26 (d, 2H, Ar—Hs, J = 8.0 Hz), 7.31 (dd, 1H, Ar—H, J = 4.2 Hz and 4.1 Hz), 7.69 (d, 2H, Ar—Hs, J = 8.2 Hz), 7.79 (dd, 1H, Ar—H, J = 2.1 Hz and 8.2 Hz), 7.96 (d, 2H, Ar—Hs, J = 8.1 Hz), 14.70 (s, 1H, NH exchanged with D_2O); ^{13}C NMR (DMSO-d_6, 100 MHz): δ 102.21, 110.57, 118.11(C≡N), 127.92, 128.27, 129.03, 130.34, 130.82, 131.72, 131.92, 133.32, 133.60, 135.55, 136.95, 145.06 (C═N), 145.43, 152.68, 159.40; Anal. Calcd for $C_{23}H_{12}Cl_2N_4S$ (447.34): C, 61.76; H, 2.70; N, 12.52. Found: C, 61.52; H, 2.84; N, 12.76; MS *m/z* (%): 446.96 (M^+, 32.50 %), 105.70 (100 %).

4.2. Biological evaluation

4.2.1. Cell culture

Three human breast cancer (BC) cell lines were used for proliferation assays: BT474, BT549, and ZR753. Lapatinib, an FDA-approved dual EGFR/HER2 inhibitor, was used as a positive control. The cell lines were sourced from ATCC (Manassas, VA), maintained at 37 °C in 5 % CO_2 and 95 % air with 100 % humidity, in RPMI-1640 or RPMI/DMEM media supplemented with 10 % heat-inactivated fetal bovine serum, L-glutamine, and 1 % penicillin/streptomycin. Cultures were kept under 20 passages and tested for Mycoplasma contamination every six months using the MycoWarning detection kit (Lonza, Switzerland).

4.1.3. Cell proliferation assay

Cell viability was assessed using the WST-8-based Cell Counting Kit-8 (Dojindo, Rockville, MD) following the manufacturer's protocol. Cells (5×10^3/well) were seeded in 96-well plates and allowed to adhere overnight. Test compounds were applied at final concentrations ranging from 0 to 50 μM (in 0.1 % DMSO). After 72 h of treatment, WST-8 reagent was added, and plates were incubated for 3 h. Absorbance was read at 450 nm using a multi-plate reader. IC_{50} values were calculated with GraphPad Prism version 5.00 (GraphPad Software, San Diego, CA).

4.1.4. In vitro antiproliferative activity of NCI-60 cell lines

In vitro Antiproliferative Activity of NCI-60 Cell Lines. The National Cancer Institute (NCI), NIH, Bethesda, MD, USA, used the Developmental Therapeutics Program (DTP) (https://dtp.cancer.gov/compsub/) to test the synthesized compounds for their cytotoxic activity against 60 cell lines of human tumors. This screen is operated using sixty distinct human tumor cell lines that correspond to leukemia, non-small cell lung cancer, colon, brain, ovarian, renal, prostate, breast, and melanoma malignancies. In order to determine the percentage of cell proliferation, the compounds are first screened at a concentration of 10 μM. Then, 6 compounds were selected for 5 doses screening. as shown in Table 1.

4.1.5. Protein kinase assays – ADP-Glo

The protein kinase assays were conducted with the Promega ADP-GloTM assay kit, which quantifies the amount of ADP produced by the protein kinase reaction. In the presence of ADP-GloTM test reagents, the kinase reaction's generation of ADP causes a rise in the luminescence signal. The protein kinase experiments were carried out in 384-well plates at 30 °C for 30 min with a final volume of 25 μl using the assay reaction protocol that follows: 5 μl of diluted active protein kinase, 5 μl of solution of substrate, 5 μl of kinase assay buffer, 5 μl of compound or 10 % DMSO, and 5 μl of ATP stock solution. The reaction mixture was first allowed to sit at room temperature in a 384-well plate for 40 min. The test was stopped by adding 5 μl of ADP-GloTM Reagent (Promega) after the incubation period. After shaking the plate, it was left to incubate at room temperature for a further forty minutes. After adding 10 μl of Kinase Detection Reagent to each well, shaking the plate, and letting it sit at room temperature for an additional 30 min, the process was completed. After that, the reaction plate was scanned using a GloMax plate reader and the ADP-GloTM Luminescence Protocol. All of the assay's components were included in the blank control setup, with the exception of the substrate (which was substituted with an equivalent volume of kinase assay buffer). Protein kinase targets' adjusted activities were calculated by subtracting the blank control value.

4.1.6. Preclinical in vivo study

Animal experiments were conducted after receiving IACUC protocol approval by the Institutional Animal Care and Use Committee of the Texas A&M University. About 6-week-old female nude mice were purchased from Envigo (Indianapolis, IN, USA). Animals were accommodated in animal house for 2 weeks before stating the experiment. About 100 μL of ZR-75-30-luciferase 2×10^6 cells mixed with Matrigel™ matrix (BD Bioscience, Frankline Lakes, NJ) were injected into the 2nd mammary gland of each mouse. Animals were divided into 3 groups with 5 mice each. After animal randomization, group 1 received a vehicle; group 2 received 10 mg/Kg interperitoneally CN32 dissolved in 10 % DMSO +10 % Tween 80, sonicate for 30 min then completed to 80 % distilled water; group 3 (positive control) received Lapatinib interperitoneally which was dissolved in 5 % DMSO +1 % Tween 80 and completed to 94 % phosphate buffer saline at pH 4 as reported [63] After 1 and 7 weeks from starting mice treatment, D-luciferin (10 μL/g body

weight) was intraperitoneally injected into each mouse, and bioluminescent images were acquired using the In Vivo Imaging System (IVIS; PerkinElmer, Waltham, MA). Recorded images are representing light intensity were generated and quantified as photons/s. Mice were weighed, and tumor volume was measured twice a week as described in our previous report [58] By the end of week 7, all mice were sacrificed, and tumor masses were excised and fixed in 10 % neutral formalin for histopathological analysis.

4.2. Molecular modeling

4.2.1. Docking

Docking studies was done for our synthesized compounds in the active site of HER2 kinase domain. Test compounds were constructed and then energy minimized using Avogadro [64]. protein structure was downloaded from protein data bank under code 3CRD. Preparation of protein and ligands was done using make receptor and make ligand tool in PyRx software [65]. Docking was done using Autodock vina [66] in a cubic grid box with side dimension of 25 Å centred on the co-crystalized ligand with exhaustiveness of 32. Final images were prepared using PyMOL software (The PyMOL Molecular Graphics System, Version 1.2r3pre, Schrödinger, LLC.).

4.2.2. Homology modeling

Missing residues of the protein data bank were constructed prior to the molecular dynamics study using homology modeling. Homology modeling was done using Swiss-Model server (https://swissmodel.expasy.org/) (60)using user template model. The full sequence of HER2 Kinase Domain Complexed with TAK-285 (PDB ID 3RCD) was downloaded as FASTA sequence from RCSB database and the pdb with missing residues was used as our template. The produced model was used without further refinement.

4.2.3. Molecular dynamics

As previously stated, GROMACS 2020.3 was used for all atom molecular dynamics simulations for the chosen protein-ligand complexes. [67,68]. In summary, topology files for the protein were generated using Charmm36 all-atom force field [69] and ligand parameterization was done using SwissParam server [70]. Complexes were assembled using ligand coordinates from co-crystallized ligand crystal structure and docking studies for compounds **3f** and **3o**. These complexes were then enclosed in a dodecahedron box and solvated with TIP3P [71] explicit water. Systems were neutralized by adding the necessary quantity of Cl- or Na + ions. Using the steepest descent algorithm, the systems energy was minimized up to a maximum force of 1000 kJ mol-1 nm-1.

After completing 1 ns of each NVT and NPT ensemble equilibration, a 100 ns production run was conducted. The V-rescale algorithm [72] maintained the temperature at 300 K, and the Parrinello-Rahman barostat [73] was used as needed to regulate the pressure. The bond's length constraints and long-range electrostatics computations were performed using the LINear Constraint Solver (LINCS) algorithm [74] and the Particle Mesh Ewald (PME) method [75], respectively. Every simulation employed a timestep of two femtoseconds. The 1.2 nm van der Waals distance cut-off (rvdw) was used. After correcting the periodic boundary condition (PBC), trajectories from the production run were analyzed using trajconv.

CRediT authorship contribution statement

Samar M. Mogheith: Writing – original draft, Visualization, Validation, Software, Methodology, Data curation. **Heba Abdelrasheed Allam:** Writing – review & editing, Writing – original draft, Validation, Supervision, Formal analysis, Conceptualization. **Manal Abdel Fattah Ezzat:** Writing – review & editing, Writing – original draft, Validation, Supervision, Investigation, Conceptualization. **Ishaq Khan:** Writing – review & editing, Writing – original draft, Methodology, Investigation, Formal analysis, Data curation. **Tamer E. Fandy:** Writing – review & editing, Writing – original draft, Methodology, Data curation. **Dalal Dawud:** Writing – review & editing, Writing – original draft, Investigation, Formal analysis, Data curation. **Zakaria Y. Abd Elmageed:** Writing – review & editing, Writing – original draft, Validation, Formal analysis, Data curation, Conceptualization. **Amgad Albohy:** Writing – review & editing, Writing – original draft, Supervision, Software, Methodology, Data curation, Conceptualization. **Hamed I. Ali:** Writing – review & editing, Writing – original draft, Supervision, Methodology, Formal analysis, Data curation, Conceptualization. **Samy Mohamady:** Writing – review & editing, Writing – original draft, Validation, Supervision, Investigation, Conceptualization.

Declaration of competing interest

The authors declare that they have no known competing financial interests or personal relationships that could have appeared to influence the work reported in this paper.

Appendix A. Supplementary data

Supplementary data for this article including characterization data and biological data, can be found online at https://doi.org/10.1016/j.bioorg.2025.108681. Crystal structures for compound 3e can be found in supplemntary material multimedia 1 and 3g in supplemntary material multimedia 2

Data availability

Data will be made available on request.

References

[1] J. Mendelsohn, J. Baselga, Status of epidermal growth factor receptor antagonists in the biology and treatment of cancer, J. Clin. Oncol. 21 (2003) 2787–2799.
[2] R. Roskoski, ErbB/HER Protein-Tyrosine Kinases: Structures and Small Molecule Inhibitors vol. 87, Pharmacological Research. Academic Press, 2014, pp. 42–59.
[3] A.J. Kay, C.P. Hunter, CDC-42 regulates PAR protein localization and function to control cellular and embryonic polarity in *C. elegans* Background: The polarization of the anterior-posterior axis (A-P) of the complex with activated Cdc42, a Rho GTPase that is implicated in the control of actin organization and cellular polarity. A role for Cdc42 in the, 2001.
[4] J. Chmielecki, J.S. Ross, K. Wang, G.M. Frampton, G.A. Palmer, S.M. Ali, et al., Cancer Diagnostics and Molecular Pathology Oncogenic Alterations in ERBB2/HER2 Represent Potential Therapeutic Targets Across Tumors From Diverse Anatomic Sites of Origin, Available from: https://doi.org/10.1634/theoncologist.2014.
[5] A. Zehir, R. Benayed, R.H. Shah, A. Syed, S. Middha, H.R. Kim, et al., Mutational landscape of metastatic cancer revealed from prospective clinical sequencing of 10,000 patients, Nat. Med. 23 (6) (2017) 703–713.
[6] T.P.J. Garrett, N.M. Mckern, M. Lou, T.C. Elleman, T.E. Adams, G.O. Lovrecz, et al., The Crystal Structure of a Truncated ErbB2 Ectodomain Reveals an Active Conformation, Poised to Interact with Other ErbB Receptors ments in anti-ErbB2 therapies are likely to flow from a better understanding of its three-dimensional (3D) struc-ture and its mechanism of action. The other members of the EGFR family are ErbB3/ HER3, which lacks a functional tyrosine kinase domain, Mol. Cell 11 (2003).
[7] W. Scheuer, T. Friess, H. Burtscher, B. Bossenmaier, J. Endl, M. Hasmann, Strongly enhanced antitumor activity of trastuzumab and pertuzumab combination treatment on HER2-positive human xenograft tumor models, Cancer Res. 69 (24) (2009) 9330–9336.
[8] Integrin-Mediated Activation of Cdc42 Controls Cell Polarity in Migrating Astrocytes through PKC.
[9] C. Marchiò, L. Annaratone, A. Marques, L. Casorzo, E. Berrino, A. Sapino, Evolving concepts in HER2 evaluation in breast cancer: heterogeneity, HER2-low carcinomas and beyond, in: Seminars in Cancer Biology. vol. 72, Academic Press, 2021, pp. 123–135.
[10] A.U. Buzdar, V. Valero, N.K. Ibrahim, D. Francis, K.R. Broglio, R.L. Theriault, et al., Neoadjuvant therapy with paclitaxel followed by 5-fluorouracil, epirubicin, and cyclophosphamide chemotherapy and concurrent trastuzumab in human epidermal growth factor receptor 2-positive operable breast cancer: an update of the initial randomized study population and data of additional patients treated with the same regimen, Clin. Cancer Res. 13 (1) (2007) 228–233.
[11] S. Ennis, D.J. Lamon, J. Rian Eyland, B.L. Ones, S.S. Teven Hak, H.F. Ank Uchs, V. P. Irginia Aton, P.D. Harm, et al., Use of chemotherapy plus a monoclonal antibody against HER2 for metastatic breast cancer that overexpresses HER2 background the

HER2 gene, which encodes the [Internet], New Engl. J. Med. 344 (2001). Available from: www.nejm.org.
[12] Smith I, Procter M, Gelber RD, Guillaume S, Feyereislova A, Dowsett M, et al. 2-year follow-up of trastuzumab after adjuvant chemotherapy in HER2-positive breast cancer: a randomised controlled trial [Internet]. Vol. 369, www.thelancet.com. 2007. Available from: www.thelancet.com.
[13] Mayo Clinic Jacksonville JNI, J. Fla, Trastuzumab plus adjuvant chemotherapy for operable HER2-positive breast cancer from the national surgical adjuvant breast and bowel project, Pittsburgh [Internet], N. Engl. J. Med. 16 (2005). Available from: www.nejm.org.
[14] M. Ferrone, S.E. Motl, Trastuzumab for the treatment of non-small-cell lung Cancer, Ann. Pharmacother. 37 (2003) 1904–1908.
[15] U. Gatzemeier, G. Groth, C. Butts, Zandwijk N. Van, F. Shepherd, A. Ardizzoni, et al., Randomized phase II trial of gemcitabine-cisplatin with or without trastuzumab in HER2-positive non-small-cell lung cancer, Ann. Oncol. 15 (1) (2004) 19–27.
[16] J.D. Berman, I.N. Leishmaniasis, K.P. Chang, R.S. Bray, M.S. Brown, S.K. Basu, et al., Studies of the HER-2/neu proto-oncogene in human breast and ovarian cancer [Internet], Trans. R. Soc. Trop. Med. Hyg. 283 (1981). CRC Press, Available from: www.sciencemag.org.
[17] A. Schneeweiss, S. Chia, T. Hickish, V. Harvey, A. Eniu, R. Hegg, et al., Pertuzumab plus trastuzumab in combination with standard neoadjuvant anthracycline-containing and anthracycline-free chemotherapy regimens in patients with HER2-positive early breast cancer: a randomized phase II cardiac safety study (TRYPHAENA), Ann. Oncol. 24 (9) (2013) 2278–2284.
[18] V. Diéras, D. Miles, S. Verma, M. Pegram, M. Welslau, J. Baselga, et al., Trastuzumab emtansine versus capecitabine plus lapatinib in patients with previously treated HER2-positive advanced breast cancer (EMILIA): a descriptive analysis of final overall survival results from a randomised, open-label, phase 3 trial, Lancet Oncol. 18 (6) (2017) 732–742.
[19] C.E. Geyer, J. Forster, D. Lindquist, S. Chan, C. Gilles Romieu, T. Pienkowski, et al., Lapatinib plus Capecitabine for HER2-Positive Advanced Breast Cancer a Bs T r Ac T [Internet], Available from: www.nejm.org, 2006.
[20] R. Nahta, F.J. Esteva, HER2 therapy: molecular mechanisms of trastuzumab resistance, Breast Cancer Res. 8 (2006).
[21] M. Scaltriti, F. Rojo, A. Ocaña, J. Anido, M. Guzman, J. Cortes, et al., Expression of p95HER2, a truncated form of the HER2 receptor, and response to anti-HER2 therapies in breast cancer, J. Natl. Cancer Inst. 99 (8) (2007) 628–638.
[22] L.V. Sequist, J.C.H. Yang, N. Yamamoto, K. O'Byrne, V. Hirsh, T. Mok, et al., Phase III study of afatinib or cisplatin plus pemetrexed in patients with metastatic lung adenocarcinoma with EGFR mutations, J. Clin. Oncol. 31 (27) (2013) 3327–3334.
[23] Fda, New Drug Therapy Approvals 2019 [Internet]., Available from: www.fda.gov.
[24] S.N. Milik, D.S. Lasheen, R.A.T. Serya, K.A.M. Abouzid, How to train your inhibitor: design strategies to overcome resistance to epidermal growth factor receptor inhibitors, Eur. J. Med. Chem. 142 (2017) 131–151. Elsevier Masson SAS.
[25] E.R. Wood, A.T. Truesdale, O.B. Mcdonald, D. Yuan, A. Hassell, S.H. Dickerson, et al., A Unique Structure for Epidermal Growth Factor Receptor Bound to GW572016 (Lapatinib): Relationships among Protein Conformation, Inhibitor Off-Rate, and Receptor Activity in Tumor Cells [Internet] vol. 64, Cancer Research, 2004. Available from: http://aacrjournals.org/cancerres/article-pdf/64/18/6652/2518347/zch01804006652.pdf.
[26] R. Roskoski, Classification of Small Molecule Protein Kinase Inhibitors Based upon the Structures of their Drug-Enzyme Complexes vol. 103, Pharmacological Research. Academic Press, 2016, pp. 26–48.
[27] J. Li, Diarrhea with HER2-targeted agents in cancer patients: a systematic review and meta-analysis, in: Journal of Clinical Pharmacology vol. 59, Blackwell Publishing Inc., 2019, pp. 935–946.
[28] S.T. Lee-Hoeflich, L. Crocker, E. Yao, T. Pham, X. Munroe, K.P. Hoeflich, et al., A central role for HER3 in HER2-amplified breast cancer: implications for targeted therapy, Cancer Res. 68 (14) (2008) 5878–5887.
[29] A.J. Jackson-Fisher, G. Bellinger, E. Shum, J.K. Duong, A.S. Perkins, M. Gassmann, et al., Formation of Neu/ErbB2-induced mammary tumors is unaffected by loss of ErbB4, Oncogene 25 (41) (2006) 5664–5672.
[30] T. Li, R. Perez-Soler, Skin toxicities associated with epidermal growth factor receptor inhibitors, Target. Oncol. 4 (2009) 107–119.
[31] B. Shuch, G. Bratslavsky, W.M. Linehan, R. Srinivasan, Sarcomatoid renal cell carcinoma: a comprehensive review of the biology and current treatment strategies, Oncologist 17 (1) (2012) 46–54.
[32] S.N. Milik, A.K. Abdel-Aziz, D.S. Lasheen, R.A.T. Serya, S. Minucci, K.A. M. Abouzid, Surmounting the resistance against EGFR inhibitors through the development of thieno[2,3-d]pyrimidine-based dual EGFR/HER2 inhibitors, Eur. J. Med. Chem. 15 (155) (2018) 316–336.
[33] S. Escrivá-de-Romaní, M. Arumí, M. Bellet, C. Saura, HER2-positive breast cancer: current and new therapeutic strategies, Breast 39 (2018) 80–88.
[34] J. Arribas, J. Baselga, K. Pedersen, J.L. Parra-Palau, p95HER2 and breast cancer, Cancer Res. 71 (2011) 1515–1519.
[35] J. Ma, H. Han, D. Liu, W. Li, H. Feng, X. Xue, et al., HER2 as a promising target for cytotoxicity T cells in human melanoma therapy, PLoS ONE 8 (8) (2013).
[36] Y. Nam, D. Hwang, N. Kim, H.S. Seo, K.B. Selim, T. Sim, Identification of 1H-pyrazolo[3,4-b]pyridine derivatives as potent ALK-L1196M inhibitors, J. Enzyme Inhib. Med. Chem. 34 (1) (2019) 1426–1438.
[37] G.D. Zhu, J. Gong, V.B. Gandhi, K. Woods, Y. Luo, X. Liu, et al., Design and synthesis of pyridine-pyrazolopyridine-based inhibitors of protein kinase B/Akt, Bioorg. Med. Chem. 15 (6) (2007) 2441–2452.
[38] J. Shi, G. Xu, W. Zhu, H. Ye, S. Yang, Y. Luo, et al., Design and synthesis of 1,4,5,6-tetrahydropyrrolo[3,4-c]pyrazoles and pyrazolo[3,4-b]pyridines for Aurora-a kinase inhibitors, Bioorg. Med. Chem. Lett. 20 (14) (2010) 4273–4278.
[39] N. Liu, Y. Wang, G. Huang, C. Ji, W. Fan, H. Li, et al., Design, synthesis and biological evaluation of 1H-pyrrolo[2,3-b]pyridine and 1H-pyrazolo[3,4-b]pyridine derivatives as c-met inhibitors, Bioorg. Chem. (65) (2016) 146–158.
[40] H. Cheng, Y. Chang, L. Zhang, J. Luo, Z. Tu, X. Lu, et al., Identification and optimization of new dual inhibitors of B-Raf and epidermal growth factor receptor kinases for overcoming resistance against vemurafenib, J. Med. Chem. 57 (6) (2014) 2692–2703.
[41] M.C. Bagley, M. Baashen, V.L. Paddock, D. Kipling, T. Davis, Regiocontrolled synthesis of 3- and 5-aminopyrazoles, pyrazolo[3,4-d] pyrimidines, pyrazolo[3,4-b]pyridines and pyrazolo[3,4-b]quinolinones as MAPK inhibitors, Tetrahedron 69 (39) (2013) 8429–8438.
[42] R.N. Misra, D.B. Rawlins, H.Y. Xiao, W. Shan, I. Bursuker, K.A. Kellar, et al., 1H-Pyrazolo[3,4-b]pyridine inhibitors of cyclin-dependent kinases, Bioorg. Med. Chem. Lett. 13 (6) (2003) 1133–1136.
[43] J.S. Duca, V.S. Madison, Insights from ab initio quantum chemical calculations into the preferred tautomeric forms and binding affinities to CDK2 of substituted pyrazolopyridines, Biopolym. - Peptide Sci. Sect. 80 (2–3) (2005) 312–318.
[44] M. Chioua, A. Samadi, E. Soriano, O. Lozach, L. Meijer, J. Marco-Contelles, Synthesis and biological evaluation of 3,6-diamino-1H-pyrazolo[3,4-b]pyridine derivatives as protein kinase inhibitors, Bioorg. Med. Chem. Lett. 19 (16) (2009) 4566–4569.
[45] P. Czodrowski, A. Mallinger, D. Wienke, C. Esdar, O. Pöschke, M. Busch, et al., Structure-based optimization of potent, selective, and orally bioavailable CDK8 inhibitors discovered by high-throughput screening, J. Med. Chem. 59 (20) (2016) 9337–9349.
[46] S. Wenglowsky, L. Ren, K.A. Ahrendt, E.R. Laird, I. Aliagas, B. Alicke, et al., Pyrazolopyridine inhibitors of B-RafV600E. Part 1: the development of selective, orally bioavailable, and efficacious inhibitors, ACS Med. Chem. Lett. 2 (5) (2011) 342–347.
[47] C.N. Joshi, D.N. Martin, J.C. Fox, N.N. Mendelev, T.A. Brown, D.A. Tulis, The soluble guanylate cyclase stimulator BAY 41-2272 inhibits vascular smooth muscle growth through the cAMP-dependent protein kinase and cGMP-dependent protein kinase pathways, J. Pharmacol. Exp. Ther. 339 (2) (2011) 394–402.
[48] B. Zhao, Y. Li, P. Xu, Y. Dai, C. Luo, Y. Sun, et al., Discovery of substituted 1H-Pyrazolo[3,4-b]pyridine derivatives as potent and selective FGFR kinase inhibitors, ACS Med. Chem. Lett. 7 (6) (2016) 629–634.
[49] D. Ramírez, M. Mejia-Gutierrez, B. Insuasty, S. Rinné, A.K. Kiper, M. Platzk, et al., 5-(Indol-2-yl)pyrazolo[3,4-b]pyridines as a new family of task-3 channel blockers: a pharmacophore-based regioselective synthesis, Molecules 26 (13) (2021).
[50] L. Gorecki, D. Muthna, S. Merdita, M. Andrs, T. Kucera, R. Havelek, et al., 7-Azaindole, 2,7-diazaindole, and 1H-pyrazole as core structures for novel anticancer agents with potential chemosensitizing properties, Eur. J. Med. Chem. (2022) 240.
[51] Q. Ye, Y. Shen, Y. Zhou, D. Lv, J. Gao, J. Li, et al., Design, synthesis and evaluation of 7-azaindazolyl-indolyl-maleimides as glycogen synthase kinase-3β (GSK-3β) inhibitors, Eur. J. Med. Chem. 68 (2013) 361–371.
[52] J. Witherington, V. Bordas, A. Gaiba, A. Naylor, A.D. Rawlings, B.P. Slingsby, et al., 6-Heteroaryl-pyrazolo[3,4-b]pyridines: potent and selective inhibitors of glycogen synthase Kinase-3 (GSK-3), Bioorg. Med. Chem. Lett. 13 (18) (2003) 3059–3062.
[53] M. Sabat, H. Wang, N. Scorah, J.D. Lawson, J. Atienza, R. Kamran, et al., Design, synthesis and optimization of 7-substituted-pyrazolo[4,3-b]pyridine ALK5 (activin receptor-like kinase 5) inhibitors, Bioorg. Med. Chem. Lett. 27 (9) (2017) 1955–1961.
[54] M.D. Hill, A multicomponent approach to highly substituted 1 H-pyrazolo[3,4-b] pyridines, Synthesis (Germany) 48 (14) (2016) 2201–2204.
[55] S. Mohamady, B. Kralt, S.K. Samwel, S.D. Taylor, Efficient one-pot, two-component modular synthesis of 3,5-disubstituted pyrazoles, ACS Omega 3 (11) (2018) 15566–15574.
[56] S. Mohamady, M.I. Ismail, S.M. Mogheith, Y.M. Attia, S.D. Taylor, Discovery of 5-Aryl-3-Thiophen-2-Yl-1H-Pyrazoles as a New Class of Hsp90 Inhibitors in Hepatocellular Carcinoma, 2019.
[57] A. Nakayama, S. Takagi, T. Yusa, M. Yaguchi, A. Hayashi, T. Tamura, et al., Antitumor activity of tak-285, an investigational, non-Pgp substrate Her2/Egfr kinase inhibitor, in cultured tumor cells, mouse and rat xenograft tumors, and in an Her2-positive brain metastasis model, J. Cancer 4 (7) (2013) 557–565.
[58] T.A. Elwaie, S.E. Abbas, E.I. Aly, R.F. George, H. Ali, N. Kraiouchkine, et al., HER2 kinase-targeted breast Cancer therapy: design, synthesis, and in vitro and in vivo evaluation of novel Lapatinib congeners as selective and potent HER2 inhibitors with favorable metabolic stability, J. Med. Chem. 63 (24) (2020) 15906–15945 [Internet]. Available from: https://doi.org/10.1021/acs.jmedchem.0c01647.
[59] Y. Ziegler, M.J. Laws, V. Sanabria Guillen, S.H. Kim, P. Dey, B.P. Smith, et al., Suppression of FOXM1 activities and breast cancer growth in vitro and in vivo by a new class of compounds, NPJ Breast Cancer 5 (1) (2019) 45 [Internet]. Available from: https://doi.org/10.1038/s41523-019-0141-7.
[60] A. Waterhouse, M. Bertoni, S. Bienert, G. Studer, G. Tauriello, R. Gumienny, et al., SWISS-MODEL: homology modelling of protein structures and complexes, Nucleic Acids Res. 46 (W1) (2018) W296–W303.
[61] A.V. Shastin, V.N. Korotchenko, V.G. Nenajdenko, E.S. Balenkova, A Novel Synthetic Approach to Dichlorostyrenes, 2024.
[62] L. Joubran, W.R. Jackson, E.M. Campi, A.J. Robinson, B.A. Wells, P.D. Godfrey, et al., Arylpropanolamines incorporating an antioxidant function as neuroprotective agents, Aust. J. Chem. 56 (6) (2003) 597–605.
[63] W.T. Hsu, C.Y. Huang, C.Y.T. Yen, A.L. Cheng, P.C.H. Hsieh, The HER2 inhibitor lapatinib potentiates doxorubicininduced cardiotoxicity through iNOS signaling, Theranostics 8 (12) (2018) 3176–3188.

[64] M.D. Hanwell, D.E. Curtis, D.C. Lonie, T. Vandermeerschd, E. Zurek, G. R. Hutchison, Avogadro: an advanced semantic chemical editor, visualization, and analysis platform, J. Chemother. 4 (8) (2012).
[65] S. Dallakyan, A.J. Olson, Small-molecule library screening by docking with PyRx, Methods Mol. Biol. 1263 (2015) 243–250.
[66] J. Eberhardt, D. Santos-Martins, A.F. Tillack, S. Forli, AutoDock Vina 1.2.0: new docking methods, expanded force field, and Python bindings, J. Chem. Inf. Model. 61 (8) (2021) 3891–3898.
[67] M.J. Abraham, T. Murtola, R. Schulz, S. Páll, J.C. Smith, B. Hess, et al., Gromacs: high performance molecular simulations through multi-level parallelism from laptops to supercomputers, SoftwareX 1–2 (2015) 19–25.
[68] M.A. Said, A. Albohy, M.A. Abdelrahman, H.S. Ibrahim, Importance of glutamine 189 flexibility in SARS-CoV-2 main protease: lesson learned from in silico virtual screening of ChEMBL database and molecular dynamics, Eur. J. Pharm. Sci. (2021) 160.
[69] J. Huang, A.D. Mackerell, CHARMM36 all-atom additive protein force field: validation based on comparison to NMR data, J. Comput. Chem. 34 (25) (2013) 2135–2145.
[70] V. Zoete, M.A. Cuendet, A. Grosdidier, O. Michielin, SwissParam: a fast force field generation tool for small organic molecules, J. Comput. Chem. 32 (11) (2011) 2359–2368.
[71] M.F. Harrach, B. Drossel, Structure and dynamics of TIP3P, TIP4P, and TIP5P water near smooth and atomistic walls of different hydroaffinity, J. Chem. Phys. 140 (17) (2014).
[72] G. Bussi, D. Donadio, M. Parrinello, Canonical sampling through velocity rescaling, J. Chem. Phys. 126 (1) (2007).
[73] M. Parrinello, A. Rahman, Polymorphic transitions in single crystals: a new molecular dynamics method, J. Appl. Phys. 52 (12) (1981) 7182–7190.
[74] B. Hess, H. Bekker, H.J.C. Berendsen, J.G.E.M. Fraaije, LINCS: a linear constraint solver for molecular simulations, in: J. Comput. Chem. vol. 18, John Wiley & Sons, Inc, 1997.
[75] T. Darden, D. York, L. Pedersen, Particle mesh Ewald: an N·log(N) method for Ewald sums in large systems, J. Chem. Phys. 98 (12) (1993) 10089–10092.